國立交通大學

物理研究所

碩 士 論 文

原子序 1 到 4 的原子基態和氫原子高階諧波產生的計算

Calculation of the Ground State of Atom Z=1-4 and High-Order Harmonic Generation for Hydrogen Atom

研 究 生：范力文

指導教授：江進福 教授

中華民國 一零三 年 七 月

原子序 1 到 4 的原子基態和氫原子高階諧波產生的計算

Calculation of the Ground State of Atom Z=1-4 and High-Order Harmonic Generation for Hydrogen Atom

研究生： 范力文　　Student： Li-Wen Fan

指導教授： 江進福　　Advisor： Tsin-Fu Jiang

國 立 交 通 大 學

物 理 研 究 所

碩 士 論 文

A Thesis

Submitted to Institute of Physics

College of Science

National Chiao Tung University

in partial Fulfillment of the Requirements

for the Degree of

Master

in

Physics

July 2014

Hsinchu, Taiwan, Republic of China

中華民國　一零三　年　七　月

原子序 1 到 4 的原子基態和氫原子高階諧波產生的計算

學生： 范力文　　指導教授： 江進福

國立交通大學　物理研究所　碩士班

摘　要

最近數十年隨著密度泛函理論(density functional theory)和電腦的發展，藉由數值方法達成原子系統相關性質的準確計算逐漸可行。本研究目標在於對原子系統基態的 Kohn-Sham 計算以及研究透過 Krieger-Li-Iafrate(KLI)程序近似最佳等效位能(optimized effective potential)對自我交互作用修正後的準確性。在基態計算的基礎上，模擬在強場下的原子系統是另一個目標。廣義擬值譜法(generalized pseudo-spectral method)是對於數值解 Kohn-Sham 方程獲得 Kohn-Sham 軌域以及數值解 Poisson 方程獲得 Hartree 位能的有效方法。對於時變計算，以分離運算子法(split operator method)處理時間算子。在結果的部分，我們先從原子序 1 到 4 以不同的交換相關泛函的 Kohn-Sham 計算獲得總能和其分量，再與前人的結果比較以驗證我們的計算可靠。再進一步，我們用 KLI 程序近似最佳等效位能並執行只有交換泛函的計算，結果顯示總能和游離能在自我交互作用修正後的準確性。最後，我們模擬在雷射場的氫原子並獲得高階諧波產生頻譜。

Calculation of the Ground State of Atom Z=1-4 and High-Order Harmonic Generation for Hydrogen Atom

Student: Li-Wen Fan Advisor: Tsin-Fu Jiang

Institute of Physics

National Chiao Tung University

ABSTRACT

The accurate calculation about properties of many-electron atomic system may be performed by numerical method in recent few decades due to the development of density functional theory and computer. The aim of the present research was to perform Kohn-Sham (KS) calculations in ground state of atomic system and investigate the accuracy of the KS calculations with optimized effective potential (OEP) approximated by Krieger-Li-Iafrate (KLI) procedure to correct the self-interaction. Based on the calculation of ground state, simulating dynamics of atomic system in intense field is the other aim. Generalized pseudo-spectral (GPS) was the useful method to numerically solve KS equation to find KS orbitals and Poisson's equation to find Hartree potential. For time-dependent calculations, spilt operator method was used to deal with the time operators. In the results section, we first obtained the total energies and their components from the KS calculations for atoms Z=1-4 with various exchange-correlation functionals and compared them with other works to make sure our calculation is reliable. Next, we performed the KS calculations with exchange-only functional and OEP approximated by KLI procedure, and we displayed the accuracy of total energies and ionization energies without self-interaction. Finally, we simulated the dynamics of a hydrogen atom in the laser field and obtained the high-order harmonic generation (HHG) spectra.

誌　　謝

感謝江進福教授這兩年多的教導，使我受益良多。此外，特別感謝李漢傑博士、唐平翰博士、鄧德明博士、鄭世達博士（按姓氏筆劃順序）在研究過程中給與我各種幫助。最後感謝家人的支持，讓我無後顧之憂，完成碩士學位。

Contents

List of Tables

List of Figures

Chapter 1

Intorduction

The fundamental works of DFT are proposed by Hohenberg and Kohn (1964) and Kohn and Sham (1965). For decades in development, DFT has become an efficient way to deal with the many-electron problem. The atomic system in stationary state has finite number of electrons and fixed configuration in stationary state. DFT is very suitable for exploring the properties of atom. We first aim to calculate the total energies and the exchange-correlation energies of neutral atoms by Kohn-Sham (KS) calculation with different exchange-correlation functionals. Comparing with other works (Davidson et al., 1991; Kurth et al., 1999), it helps to establish the reliable KS calculation.

The exactly exchange-correlation functional is not yet known, so the approximation of exchange-correlation energy functionals is always one of the notable issues in DFT. The local spin-density approximation (LSDA) is widely employed. However, it has self-interaction such that the long-range behavior is not correct. The one of subjects in the present research is the correction to the self-interaction by the optimized effective potential (OEP) method and Krieger-Li-Iafrate (KLI) approximation (Krieger et al., 1992a). Based on the reliable KS calculation, we can establish the advanced techniques, OEP method and KLI approximation, and carry out the correctly total energies and highest occupied orbital energies for atomic system.

When an atomic or molecule system in intense field, the electronic response is highly non-linear. The non-linear process displays many interesting phenomena and applications. One consequence of them is the high-order harmonic generation (HHG) which converts the frequency of intense field into many integer multiples of the frequency. HHG spectra generally consist of a sharp decline, a plateau in which the harmonic intensity varies

weakly, and a sharp cut-off (see Figure 4.2.3). The maximum energy of harmonic photon is given by the cut-off law (Krause et al., 1992).

$$E_{cut} \approx E_I + 3.17U_p \tag{1.0.1}$$

where E_I is ionization energy, and U_p is the pondermotive energy. The high-order harmonic generation (HHG) is established as one of the best way to produce ultrashort coherent light (Midorikawa, 2011). It is worth researching with a theoretical aspect. In the present research, the other subject is the simulation of HHG of a hydrogen atom in the intense field. We directly solve the time-dependent Schrödinger equation to find the evolution of wave function and remark some features about HHG from the results. The results are also compared with the work (Tong and Chu, 1997b) to confirm the result. It is to build up our ability to deal with the time-dependent problems.

With the development of computer, the new device, graphics processing unit (GPU) accelerator and programming interface, OpenACC, are used in our computation. We perform the computation for the time iteration to simulate the HHG of a hydrogen atom in the intense field. It has an apparent effect on the computational speed, and the cost time is reduced to the acceptable range.

The necessarily numerical method for the present research are introduced in Chapter 2. Chapter 3 is a brief about density functional theory for the KS calculation. The result and discussion are in Chapter 4. From now on all of equations are in atomic unit. Following four fundamental constants are unity.

$$\hbar = e = m_e = \frac{1}{4\pi\varepsilon_0} = 1 \tag{1.0.2}$$

Chapter 2

Methods

2.1 Quadratures and Grids

The integrations occur frequently in the inner product of two wave functions or an expansion in orthogonal basis. Its specific and non-uniform grids are also used in the generalized-pseudo spectral method throughout the numerical calculations in the present research. To numerical calculate these integrations, the quadrature and specific grids are necessary. Gauss-Legendre quadrature and Gauss-Legendre-Lobatto quadrature are introduced in this section.

2.1.1 Gaussian Quadrature

For the numerical integration, Gaussian quadrature has the highest accuracy in theory, but its grids and coefficients are hard to calculate. The general formula of Gaussian quadrature is

$$\int_a^b w(x)f(x)dx = \sum_i W_i f(x_i) \tag{2.1.1}$$

where $w(x)$ is the weighting function, x_i are specific grids called **Gauss nodes** or **Gaussian grids**, and W_i are the weights on the Gaussian grids. When the interval $[a, b]$ and weighting function $w(x)$ are given, the W_i and x_i are determined.

There are many typical forms for the interval $[a, b]$ and weighting function $w(x)$ derived from different orthogonal polynomials in (2.1.1). For a example, the interval $[-1, 1]$ and weighting function $1/\sqrt{1-x^2}$ in common use are derived from Chebyshev polynomials of the first kind.

2.1.2 Gaussian Grids and Weights

We only chose the $[a, b]$ and $w(x)$ based on the Legendre polynomials throughout the present research. For Legendre polynomials, the valid interval is $[-1, 1]$. The weighting function $w(x)$ is a constant as follow

$$w(x) = 1 \tag{2.1.2}$$

In practice, the unity lets us avoid calculating the weighting function for the integral function. With the given interval $[-1, 1]$ and weighting function $w(x)$, there are three unique sets of Gaussian grids x_i and weights W_i. We used two of them in calculation.

The first set is the roots of Legendre polynomial $P_N(x)$, $x = \cos\theta$, with degree N. The roots can be numerically calculated by the recurrence relations, (A.0.3) and (A.0.4), and Newton's method. The roots of $P_N(x)$ form following collocation points,

$$x_i \in \{x_1, x_2, \ldots, x_{N-1}, x_N\}. \tag{2.1.3}$$

In this thesis, the set (2.1.3) of points is called **Gauss-Legendre** grids, abbreviated to GL grids. They are non-uniformly distributed over the abscissa and symmetric (or antisymmetry) to zero point. The relation between the polynomial degree N and the number of GL grids N_{GL} is

$$N_{GL} = N \tag{2.1.4}$$

The weights W_i for GL grids are (Abramowitz and Stegun, 1972, p.887)

$$W_i = \frac{2}{(1 - x_i)[P'_N(x)]^2} \tag{2.1.5}$$

The domain of GL grids is $[-1, 1]$. It is suitable for expressing the polar angle in spherical coordinate in discreteness without mapping.

The other set is the roots of the first derivative of Legendre polynomial $P'_N(x)$, $x = \cos\theta$, with degree N. The roots can be numerically calculated by recurrence relations, (A.0.4) and (A.0.5) and Newton's method. In addition, it includes the end points of interval $[-1, 1]$. The roots and end points form the collocation points,

$$x_i \in \{x_0 = -1, x_1, x_2, \ldots, x_{N-1}, x_N = 1\} \tag{2.1.6}$$

where x_0 and x_N are end points, and $x_1, \cdots, x_{N-1}$ are the roots of $P'_N(x)$. In this thesis, the set (2.1.6) is called **Gauss-Legendre-Lobatto** grids, abbreviated to GLL grids.

Their distribution is the same as GL grid. The relation between the polynomial degree N and the number of GLL grids N'_{GLL} is

$$N'_{GLL} = N + 1. \tag{2.1.7}$$

The weights W_i for GLL grids are (Abramowitz and Stegun, 1972, p.888)

$$W_i = \frac{2}{N(N+1)[P_N(x_i)]^2}. \tag{2.1.8}$$

Because of the inaccuracy close to the end points of interval, the subset of GLL grids was used more often than the GLL grids in actual calculation. The subset excluding the end points, x_0 and x_N, only has the roots of $P'_N(x)$,

$$x_i \in \{x_1, x_2, ..., x_{N-1}\}. \tag{2.1.9}$$

The relation between the polynomial degree N, the number of all GLL grids N'_{GLL}, and the number of this subset N_{GLL} is

$$N_{GLL} = N - 1 = N'_{GLL} - 2. \tag{2.1.10}$$

2.1.3 Mapping Funciton

The GLL grids x_i of which valid domain is $[-1, 1]$ can not express the radius r of which valid domain is $[0, \infty]$ in spherical coordinates. The connection of different domain is called **mapping**. To achieve mapping, it requires a function which is also called **mapping function**.

Between the two intervals, $x \in [-1, +1]$ and $r \in [0, \infty]$, there are two nonlinear mapping, **algebraic mapping** and **exponential mapping**, to use. We only used algebraic mapping in the present research because the algebraic mapping is more accurate than exponential mapping in practice. The algebraic mapping is

$$r(x) = L\frac{1 + x + \beta}{1 - x + \alpha} \tag{2.1.11}$$

where α and β are constants to determine the boundaries, r_{min} and r_{max}. With $x = -1$, $r(-1)$ is the boundary r_{min},

$$r_{min} = L\frac{\beta}{2 + \alpha}. \tag{2.1.12}$$

With $x = 1$, $r(1)$ is the boundary r_{max},

$$r_{max} = L\frac{2 + \beta}{\alpha}. \tag{2.1.13}$$

When $\alpha = \beta = 0$, the interval $[-1, 1]$ can be map to the interval $[0, \infty]$.

The values of two constants α and β in (2.1.11) should be noted. The constant β may not be used and let itself be zero.

$$\beta = 0 \tag{2.1.14}$$

The other constant α should be added and let itself be non-zero to avoid divergence of $r(x)$ at the last GLL point, $r(1)$. $r(x)$, r_{min}, and r_{max} with the given β are redefined as

$$r(x) = L\frac{1+x}{1-x+\alpha} \tag{2.1.15}$$

$$r_{min} = 0 \tag{2.1.16}$$

$$r_{max} = L\frac{2}{\alpha} \tag{2.1.17}$$

The other constant L in mapping functions, (2.1.11) and (2.1.15), is called **length scale**. L affects the distribution of all collocation points, and it is important to accurately calculate. Figure 2.1.1 shows how to change the distribution of 22 GLL grids by mapping function with various L in a fixed range $[0, r_{max}] = [0, 100]$. There are nine horizontal lines for nine distributions by mapping function with nine length scales.

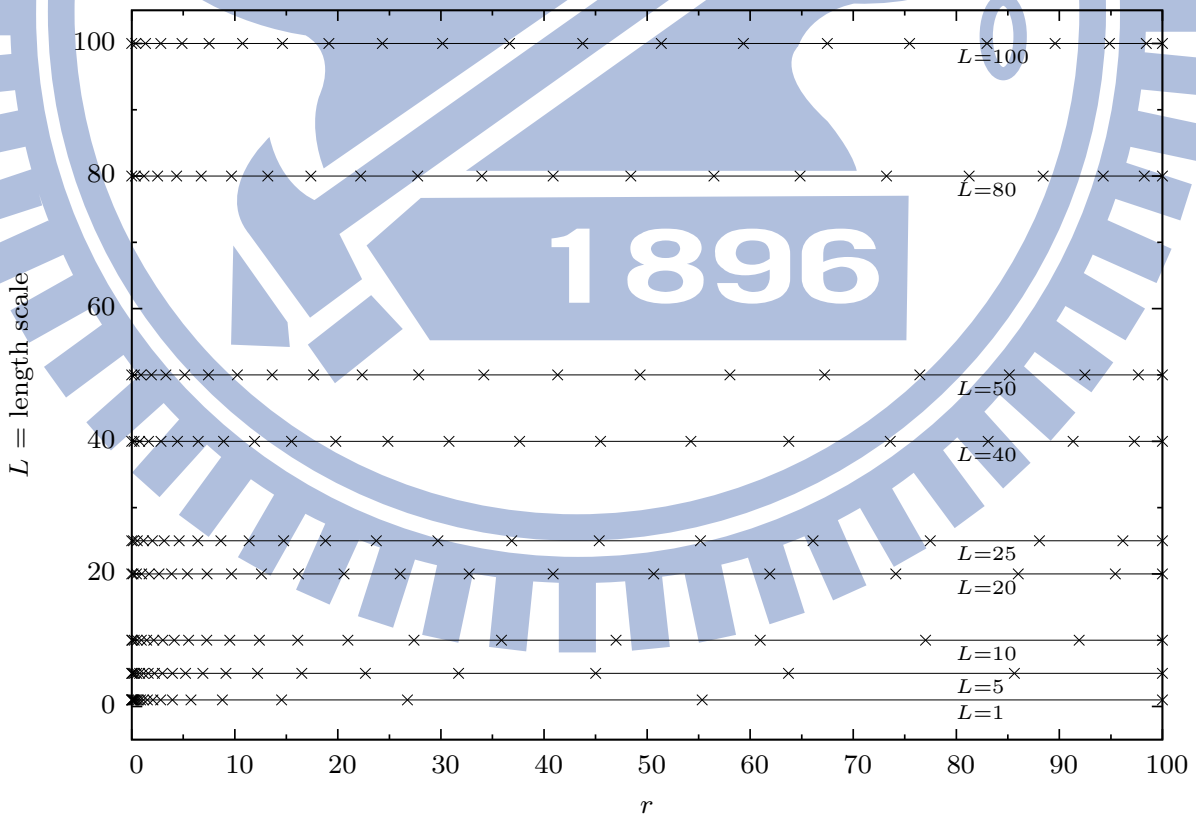

Figure 2.1.1: Influence of various length scale L by mapping function on grid-point distribution

$L = 1$ does not change the distribution. The distribution shows that the most grids are close to the origin, $r = 0$, and very dense near the origin, $r = 0$. It can not correctly describe the shape of a function on the middle or far grids, and it may lead to inaccuracy calculation when $L = 1$. On increase of L, the influence of L on the distribution decreases gradually, and the distribution is changed a little. When L is over a value, the grids start to approach to the r_{max}.

In practice, the length scale L depends on the variation of function. With the adapted length scales for different problems, the grids can describe the functions well. In the present research, the most functions are the wave functions in stationary state. The wave functions oscillate near the nucleus and decay quickly, so we multiplied $r_{max}/5$ or $r_{max}/10$ to the mapping function $r(x)$ as a length scale.

Map the interval $[-1, 1]$ to interval $[0, r_{max}]$ by the mapping function (2.1.15), and the Gaussian quadrature requires a variable change,

$$r'(x) = \frac{d}{dx} r(x) = L \frac{2 + \alpha}{(1 - x + \alpha)^2}, \tag{2.1.18}$$

in term of x to work. The Gaussian quadrature with interval $[-1, 1]$ and weighting function $w(x) = 1$ becomes

$$\int_0^{r_{max}} f(r) dr = \sum_i W_i f(r(x_i)) \frac{dr(x_i)}{dx}. \tag{2.1.19}$$

where x_i are GLL or GL grids, W_i are weights on GLL or GL grids.

More mapping functions that map finite interval to semi-infinite interval or infinite interval can be found in Canuto et al. (2007, § 8.8)

2.2 Generalized Pseudo-Spectral Method (GPS)

Generalized pseudo-spectral method (GPS) is to solve the ordinary differential equations (ODE) or partial differential equations (PDE). GPS uses a pseudo-spectral basis which is constructed by orthogonal polynomials to represent the functions in a differential equation on Gaussian grids. By GPS, ODE becomes an integration or eigenvalue problem. On the Gaussian grids and pseudo-spectral basis, it is easy to deal with the integration and eigenvalue problem. GPS plays a key role in the present research. This section and the next two sections provide the principles and its applications.

2.2.1 Polynomial Interpolation and Cardinal Functions

Polynomial interpolation is one of interpolations methods. It is the generalization of linear interpolation which is the simplest interpolation. The Lagrange interpolation is one of algorithms to realize polynomial interpolation and better than other algorithms in time complexity.

The Lagrange interpolation is known that a unknown function $f(x)$ with some given points x_i is approximated by a polynomial $p(x)$. In general, if there are $N+1$ given points, the unknown function $f(x)$ is fitted by a degree-N polynomial $p_N(x)$ as follow

$$f(x) \approx p_N(x) = \sum_{i=0}^{N} f(x_i) g_i(x) \tag{2.2.1}$$

where $g_i(x)$ are cardinal functions. With these given points x_j, the cardinal functions are defined by

$$g_i(x) = \prod_{\substack{j=0 \\ j \neq i}}^{N} \frac{x - x_j}{x_i - x_j}. \tag{2.2.2}$$

In definition, it must satisfy following property,

$$g_j(x_i) = \delta_{ij}. \tag{2.2.3}$$

The Lagrange interpolation with the given cardinal functions is also called **cardinal expansion** or **expansion in cardinal functions**. The cardinal functions defined by orthogonal polynomials form the pseudo-spectral basis.

2.2.2 Cardinal Functions for Orthogonal Polynomials

By GLL grids and Legendre polynomials, define the cardinal functions $g_j(x)$ as follow (Canuto et al., 1988, p.64)

$$g_j(x) = -\frac{1}{N(N+1)P_N(x_j)}\frac{(1-x^2)P'_N(x)}{x-x_j} \tag{2.2.4}$$

Following paragraphs show that the cardinal functions (2.2.4) have the property (2.2.3).

When $x = x_i = x_j$ on GLL grids, use a limit to approach.

$$\lim_{x\to x_i} g_j(x) = -\frac{1}{N(N+1)P_N(x_j)}\frac{(1-x_j^2)P'_N(x_j)}{x_j-x_j} \tag{2.2.5}$$

See both denominator and numerator are zero, so apply l'Hôpital's rule to the limit.

$$\lim_{x\to x_i} g_j(x) = -\frac{1}{N(N+1)P_N(x_j)}\frac{[(1-x^2)P'_N(x)]'}{(x-x_j)'} \tag{2.2.6}$$

With the relation (A.0.6) in appendix A,

$$\lim_{x\to x_i} g_j(x) = -\frac{1}{N(N+1)P_N(x_j)}\frac{[-N(N+1)P_N(x)]}{1}. \tag{2.2.7}$$

The limit is a constant.

$$g_j(x_j) = -\frac{1}{N(N+1)P_N(x_j)}\frac{[-N(N+1)P_N(x_j)]}{1} = 1 \tag{2.2.8}$$

When $x = x_i \neq x_j$ on GLL grids,

$$g_j(x_i) = -\frac{1}{N(N+1)P_N(x_j)}\frac{(1-x_i^2)P'_N(x_i)}{x_i-x_j} \tag{2.2.9}$$

Only the numerator is zero because $(1-x_i^2) = 0$, or $P'_N(xi) = 0$, and the other coefficients are not zero.

$$g_j(x_i) = -\frac{1}{N(N+1)P_N(x_j)}\frac{0}{x_i-x_j} = 0 \tag{2.2.10}$$

Combine two results, (2.2.8) and (2.2.10), and the cardinal functions satisfy the property (2.2.3).

2.2.3 Derivatives of Cardinal Functions

The cardinal expansion lets the operators in differential equation work on the cardinal functions to represent the operators in discrete variables. For the cardinal functions (2.2.4), its first and second derivatives which we applied in practice are analysed (Wang and Yan, 2012) and summarized (Telnov and Chu, 1999, appendix) in this subsection.

I From definition (2.2.4),

$$N(N+1)P_N(x_j)(x-x_j)g_j(x) = -(1-x^2)P'_N(x). \tag{2.2.11}$$

Differentiate both sides with respect to x.

$$N(N+1)P_N(x_j)g_j(x) + N(N+1)P_N(x_j)(x-x_j)\frac{dg_j(x)}{dx} = -\frac{d}{dx}[(1-x^2)P'_N(x)] \tag{2.2.12}$$

Replace $[(1-x^2)P'_N(x)]'$ by (A.0.6).

$$N(N+1)P_N(x_j)g_j(x) + N(N+1)P_N(x_j)(x-x_j)\frac{dg_j(x)}{dx} = N(N+1)P_N(x) \tag{2.2.13}$$

Eliminate the coefficient $N(N+1)$ occurring on both sides.

$$P_N(x_j)g_j(x) + P_N(x_j)(x-x_j)\frac{dg_j(x)}{dx} = P_N(x) \tag{2.2.14}$$

When $x = x_i \neq x_j$ on GLL grids,

$$P_N(x_j)g_j(x_i) + P_N(x_j)(x_i-x_j)\frac{dg_j(x_i)}{dx} = P_N(x_i). \tag{2.2.15}$$

$g_j(x_i) = 0$ because $x_i \neq x_j$, and rearrange the equation.

$$\frac{dg_j(x_i)}{dx} = \frac{1}{(x_i-x_j)}\frac{P_N(x_i)}{P_N(x_j)} \tag{2.2.16}$$

II Take the derivatives of the terms on both sides of (2.2.14) with respect to x.

$$2P_N(x_j)\frac{dg_j(x)}{dx} + P_N(x_j)(x-x_j)\frac{d^2g_j(x)}{dx^2} = P'_N(x) \tag{2.2.17}$$

When $x = x_i = x_j$ on GLL grids, and $x \neq x_0 \neq x_N$,

$$2P_N(x_j)\frac{dg_j(x_j)}{dx} + P_N(x_j)(x_j-x_j)\frac{d^2g_j(x_j)}{dx^2} = P'_N(x_j). \tag{2.2.18}$$

$(x_j - x_j)$ and $P'_N(x_j)$ are zero, and $P_N(x_j)$ is not zero.

$$\frac{dg_j(x_j)}{dx} = 0 \tag{2.2.19}$$

III When $x = x_i = x_j = x_0 = -1$ on GLL grids, from (2.2.17),

$$2P_N(-1)\frac{dg_j(-1)}{dx} + P_N(-1)(-1+1)\frac{d^2g_j(-1)}{dx^2} = P'_N(-1) \tag{2.2.20}$$

The second term is zero, and the $P_N(\pm 1)$ and $P'_N(\pm 1)$ are given by (A.0.1) and (A.0.2) in Appendix A.

$$2(-1)^N\frac{dg_j(x_0)}{dx} + 0 = (-1)^{N+1}\frac{N(N+1)}{2} \tag{2.2.21}$$

Rearrange the equation.

$$\frac{dg_j(x_0)}{dx} = -\frac{N(N+1)}{4} \tag{2.2.22}$$

When $x = x_i = x_j = x_N = 1$ on GLL grids, by the same way,

$$\frac{dg_j(x_N)}{dx} = \frac{N(N+1)}{4} \tag{2.2.23}$$

Following equation summarizes the formulae, (2.2.16), (2.2.19), (2.2.22), and (2.2.23), of the first derivative of the $g_j(x)$ on GLL grids.

$$\frac{dg_j(x_i)}{dx} = g'_j(x_i) = d'_{ij}\frac{P_N(x_i)}{P_N(x_j)} \tag{2.2.24}$$

where

$$d'_{ij} = \begin{cases} \dfrac{1}{x_i - x_j} & i \neq j \\ 0 & i = j \neq 0 \neq N \\ -\dfrac{N(N+1)}{4} & (i,j) = (0,0) \\ \dfrac{N(N+1)}{4} & (i,j) = (N,N) \end{cases} \tag{2.2.25}$$

The calculation of the second derivative of the $g_j(x)$ on GLL grids based on its first derivative on GLL grids. Following paragraphs are the derivation of the formulae for the second derivative of $g_j(x)$ on GLL grids.

I When $x = x_i \neq x_j$ on GLL grids, and $x_i \neq 0 \neq N$, from (2.2.17),

$$2P_N(x_j)\frac{dg_j(x_i)}{dx} + P_N(x_j)(x_i - x_j)\frac{d^2g_j(x_i)}{dx^2} = P'_N(x_i). \tag{2.2.26}$$

$P'_N(x_i)$ is zero, and the $g'_j(x_i)$ where $x_i \neq x_j$ is given by (2.2.16).

$$\frac{2P_N(x_i)}{x_i - x_j} + P_N(x_j)(x_i - x_j)\frac{d^2g_j(x_i)}{dx^2} = 0 \tag{2.2.27}$$

Rearrange the equation.

$$\frac{d^2g_j(x_i)}{dx^2} = -\frac{2}{(x_i - x_j)^2}\frac{P_N(x_i)}{P_N(x_j)} \tag{2.2.28}$$

II Differentiate both sides of (2.2.17) with respect to x.

$$3P_N(x)\frac{d^2g_j(x)}{dx^2} + (x - x_j)P_N(x_j)\frac{d^3g_j(x)}{dx^3} = P'_N(x) \tag{2.2.29}$$

When $x = x_i = x_j$ on GLL grids, $x_i = x_j \neq x_0$, and $x_i = x_j \neq x_N$,

$$3P_N(x_j)\frac{d^2g_j(x_j)}{dx^2} + (x_j - x_j)P_N(x_j)\frac{d^3g_j(x_j)}{dx^3} = P'_N(x_j). \tag{2.2.30}$$

The second term is zero because of its coefficient, $(x_j - x_j) = 0$. With the relation (A.0.10) in Appendix A,

$$3P_N(x_j)\frac{d^2 g_j(x_j)}{dx^2} + 0 = \frac{N(N+1)P_N(x_j)}{(x_j^2 - 1)}. \tag{2.2.31}$$

Rearrange the equation.

$$\frac{d^2 g_j(x_j)}{dx^2} = \frac{N(N+1)}{(x_j^2 - 1)}\frac{P_N(x_j)}{P_N(x_j)} = -\frac{N(N+1)}{3(1 - x_j^2)} \tag{2.2.32}$$

Following equation summarizes the formulae, (2.2.28), (2.2.32), and remaining formulae that we did not use in the present research.

$$\frac{d^2 g_j(x_i)}{dx} = g_j''(x_i) = d_{ij}''\frac{P_N(x_i)}{P_N(x_j)} \tag{2.2.33}$$

where

$$d_{ij}'' = \begin{cases} -\dfrac{2}{(x_i - x_j)^2} & i \neq j \quad (i,j) \neq (0,N) \neq (N,0) \\ -\dfrac{N(N+1)}{3(1 - x_j^2)} & i = j \quad (i,j) \neq (0,0) \neq (N,N) \\ \dfrac{N(N+1) - 2}{4} & (i,j) = (0,N) = (N,0) \\ \dfrac{N(N+1)[N(N+1) - 2]}{24} & (i,j) = (0,0) = (N,N) \end{cases} \tag{2.2.34}$$

Pseudo-spectral methods are closely related to the spectral methods. The famous publications, Peyret (2002) and Canuto et al. (2007), about spectral methods also offer the materials for pseudo-spectral methods.

2.2.4 Differential Matrix

(2.2.24) points out a direct application to numerical differential. Assume that $f(r(x))$ is a function which maps from the r domain to the x domain. Take the derivative with respect to r.

$$\frac{df(r(x))}{dr} = \frac{dx}{dr(x)}\frac{df(r(x))}{dx} \tag{2.2.35}$$

Expand $f(x)$ in the cardinal functions (2.2.4).

$$\frac{df(r(x))}{dr} = \frac{1}{r'(x)}\sum_j \frac{dg_j(x)}{dx} f(r(x_j)) \tag{2.2.36}$$

Discretize x on GLL grids, $x = x_i$.

$$\frac{df(r(x_i))}{dr} = \frac{1}{r'(x_i)}\sum_j \frac{dg_j(x_i)}{dx} f(r(x_j)) \tag{2.2.37}$$

Equation (2.2.37) is a matrix-vector product. With all GLL grids, x_i and x_j, the $g'_j(x_i)$ with the coefficient $[r'(x_i)]^{-1}$ form a $(N+1)\times(N+1)$ matrix D. The element D_{ij} of the matrix D is

$$D_{ij} = \frac{1}{r'(x_i)}\frac{dg(x_i)}{dx} = \frac{1}{r'(x_i)}d'_{ij}\frac{P_N(x_i)}{P_N(x_j)} \tag{2.2.38}$$

where d'_{ij} is given by (2.2.25). If $f(r(x_i))$ is given, the matrix-vector product of D_{ij} and $f(r(x_j))$ can directly give the derivatives $f'(r(x_i))$ with respect to r without other techniques. The work of D is the same as a differential operator, and D is called **differential matrix**.

When more grids are used in a numerical calculation, more round-errors occur in numerically calculating the derivatives by the differential matrix D. Bayliss et al. (1995) offer a technique to reduce the round-off errors to make the derivatives more accurate. It is easy to derive the technique. Let a operator d/dx work on a constant function, $f(x) = c$ where c is a constant.

$$\frac{d}{dx}f(x) = \frac{d}{dx}c = 0 \tag{2.2.39}$$

Discretize x on GLL grids, and substitute the operator by the differential matrix D.

$$\sum_j D_{ij}f(x_j) = 0 \tag{2.2.40}$$

Let the diagonal elements of D be *correction* terms.

$$D_{ii}f(x_i) = -\sum_{\substack{j\\ i\neq j}} D_{ij}f(x_j) \tag{2.2.41}$$

Divide both sides by c, and the diagonal elements now become

$$D_{ii} = -\sum_{\substack{j\\ j\neq i}} D_{ij}. \tag{2.2.42}$$

The off-diagonal elements follow the original definition. The diagonal elements (2.2.42) eliminate the round-off errors of the off-diagonal elements. The differential matrix with the correction is denoted D^{cor}.

For an example of which derivative is analysis and easy to calculate,

$$f(r(x)) = \exp(-r(x)). \tag{2.2.43}$$

We numerically calculated its first and second derivative with respect to r by the differential matrix D.

By the mapping function (2.1.15) with $L = 20$, the valid interval of r is $[0, 200]$. 21 GLL grids are used in the numerical calculation, and 21 derivatives are numerically calculated by method 1 and method 2. For the numerical differential, the method 1 is the matrix-vector product of the differential matrix D and f, and the method 2 is the matrix-vector product of the differential matrix D^{cor} and f. The second derivatives are numerically calculated by the matrix-vector product again. The relative errors of the first derivative f' and second derivatives f'' on 21 GLL grids are represented in Table 2.2.1. It is suitable to remark some properties of the differential matrix and GPS.

Table 2.2.1: Relative errors of the first derivatives and second derivatives numerically calculated by method 1 and method 2 on 21 GLL grids.

i	$r(x_i)$	Method 1		Method 2		$f(r) = e^{-r}$
		f'	f''	f'	f''	
0	0.00	5.00[−09]	1.06[−07]	5.00[−09]	1.06[−07]	1.00[+00]
1	0.16	−2.28[−09]	4.55[−09]	−2.28[−09]	4.55[−09]	8.52[−01]
2	0.54	2.27[−09]	−4.81[−09]	2.27[−09]	−4.81[−09]	5.82[−01]
3	1.16	−3.01[−09]	7.07[−09]	−3.01[−09]	7.07[−09]	3.13[−01]
4	2.04	4.93[−09]	−1.40[−08]	4.93[−09]	−1.40[−08]	1.30[−01]
5	3.23	−9.45[−09]	3.80[−08]	−9.45[−09]	3.80[−08]	3.95[−02]
6	4.78	1.64[−08]	−1.49[−07]	1.64[−08]	−1.49[−07]	8.42[−03]
7	6.76	5.54[−08]	9.02[−07]	5.54[−08]	9.02[−07]	1.16[−03]
8	9.29	−2.43[−06]	−9.45[−06]	−2.43[−06]	−9.45[−06]	9.19[−05]
9	12.53	9.09[−05]	1.98[−04]	9.09[−05]	1.98[−04]	3.63[−06]
10	16.67	−6.53[−03]	−1.01[−02]	−6.53[−03]	−1.01[−02]	5.78[−08]
11	22.02	1.35[+00]	1.69[+00]	1.35[+00]	1.69[+00]	2.74[−10]
12	29.00	−1.27[+03]	−1.39[+03]	−1.27[+03]	−1.39[+03]	2.55[−13]
13	38.21	1.03[+07]	1.03[+07]	1.03[+07]	1.03[+07]	2.54[−17]
14	50.49	−1.67[+12]	−1.59[+12]	−1.67[+12]	−1.59[+12]	1.18[−22]
15	66.97	1.70[+19]	1.59[+19]	1.70[+19]	1.59[+19]	8.27[−30]
16	88.91	−4.04[+28]	−3.74[+28]	−4.04[+28]	−3.74[+28]	2.43[−39]
17	117.20	5.51[+40]	5.09[+40]	5.51[+40]	5.09[+40]	1.26[−51]
18	150.53	−1.26[+55]	−1.16[+55]	−1.26[+55]	−1.16[+55]	4.24[−66]
19	182.37	7.98[+68]	7.39[+68]	7.98[+68]	7.39[+68]	6.30[−80]
20	200.00	−7.60[+76]	−5.59[+76]	−7.60[+76]	−5.59[+76]	1.38[−87]

The relative errors on the far grids are huge. When r is large, the tiny values are hard to be described by the pseudo-spectral basis. It does not affect the numerical calculation because the order of magnitude is too small. If the cases is that $\exp(-r)$ fast decay when r increase, the values on the grids near the point, $r = 0$, are leading terms, and the values on the grids far from the point, $r = 0$, can be ignored.

As listed in Table 2.2.1, the first derivatives f' and second derivatives f'' numerically calculated by the method 1 and 2 are almost identical to each other. It is evident that the accuracy of f'' is less than the accuracy of f' especially at the point $r(x_0)$. The round-off errors occurring near the boundary are more than in the middle as same as the result

of Bayliss et al. (1995). The correction to round-off errors on the less grids is not easily obvious in Table 2.2.1.

To show the efficacy of the technique for reducing the round-off errors, we present the relative errors of the first derivative f' and second derivative f'' numerical calculated by method 1 and method 2 at the point $r(x_0)$, $r(x_0) = 0$, of various number of GLL grids in Table 2.2.2. We used the mapping function (2.1.15) with length scale $L = 20$ to map r domain $[0, 200]$ to x domain $[-1, 1]$ in the calculation for Table 2.2.2. The method 1 and method 2 are the same as the method 1 and method 2 in Table 2.2.1. The exact values of f' and f'' at the point $r(x_0)$ are -1 and 1.

Table 2.2.2: Relative errors of the first and second derivatives individually evaluated by method 1 and method 2 at the first point $r(x_0) = 0$ of various numbers of GLL grid.

N_{GLL}	Method 1		Method 2	
	f'	f''	f'	f''
21	5.00[−09]	1.06[−07]	5.00[−09]	1.06[−07]
51	8.49[−13]	1.13[−10]	−1.79[−14]	−1.05[−13]
103	9.55[−14]	−2.85[−10]	−1.82[−14]	−3.21[−11]
203	4.21[−10]	6.16[−07]	1.43[−13]	−7.68[−11]
403	−2.02[−09]	−1.19[−05]	−2.91[−13]	−2.34[−09]

As listed in Table 2.2.2, the relative errors of f' and f'' evaluated by method 1 increase considerably from $N_{GLL} = 51$ to $N_{GLL} = 403$ by $4 - 5$ orders of magnitude. The increase in relative errors indicates that the results have more the round-off error when more grids are used. The f'' evaluated by method 1 only has 4 significant figures behind the decimal point if we use 403 GLL grids.

By method 2, the first derivatives f' have about $12 - 13$ significant figures behind the decimal point. They almost arrive the maximum accuracy of a double-precision number in programming. The method 2 also reduce the relative errors of f'' significantly while they could not arrive the maximum precision of double-precision number. The f'' evaluated by method 2 with 403 grids only remain 8 significant figures behind decimal point, so the number of grid should be adequate. On the whole, the technique offered by Bayliss et al. (1995) has beneficial effect on reducing the round-off errors.

2.3 Application of GPS to Schrödinger Equation

The time-independent Schrödinger equation, which is abbreviated to SE, reads

$$\hat{H}\psi(\mathbf{r}) = -\frac{\hbar^2}{2m}\nabla^2\psi(\mathbf{r}) + V\psi(\mathbf{r}) = E\psi(\mathbf{r}) \quad (SI). \tag{2.3.1}$$

Suppose the external potential V only depends on radius r in spherical coordinates. By separation of variables and variable change, $u(r) = rR(r)$, the radial equation in atomic unit is

$$-\frac{1}{2}\frac{d^2}{dr^2}u(r) + [\frac{l(l+1)}{2r^2} + V(r)]u(r) = Eu(r). \tag{2.3.2}$$

By the expansion in spherical harmonics, we only solved the radial equation.

The first application of GPS is a solver for Schrödinger equation. In this section, remove the undesirable feature due to the non-linear mapping at first, and construct the Hamiltonian matrix by GPS. The technique to symmetrize the Hamiltonian matrix is also introduced in this section. We solved the SE of a hydrogen atom in the last subsection.

2.3.1 Radial Equation Represented in x Domain

For the application of GPS, discretize $u(r)$ on the GLL grids by the mapping function (2.1.15). The non-linear mapping of the second derivative of $u(r(x))$ with respect to r leads to the first derivative of $u(r(x))$ with respect to x occurring in the radial equation. The elimination of the undesirable first derivative with respect to x is necessary for symmetrizing the Hamiltonian matrix. This subsection represents how to eliminate the redundant derivative.

Mapping $u(r)$ from r domain to x domain, the first derivative of $u(r)$ with respect to r is

$$\frac{d}{dr}u(r(x)) = \frac{dx}{dr}\frac{d}{dx}u(r(x)) = \frac{1}{r'}\frac{d}{dx}u(r(x)). \tag{2.3.3}$$

Take a derivative of the terms on both sides with respect to r again.

$$\frac{d^2}{dr^2}u(r(x)) = \frac{1}{(r')^2}[-\frac{r''}{r'}\frac{d}{dx} + \frac{d^2}{dx^2}]u(r(x)) \tag{2.3.4}$$

With (2.3.4), the radial equation (2.3.2) becomes

$$\frac{1}{2(r')^2}[-\frac{r''}{r'}\frac{d}{dx} + \frac{d^2}{dx^2}]u(r(x)) + [\frac{l(l+1)}{2r^2} + V(r)]u(r(x)) = Eu(r(x)). \tag{2.3.5}$$

To eliminate the first derivative, the variable change makes

$$u(r) = (\frac{dr(x)}{dx})^C f(x) = (r')^C f(x) \tag{2.3.6}$$

where the $f(x)$ is a function which can be expanded in the cardinal functions (2.2.4) in x domain, and the exponent C is a undetermined coefficient. Determine C by substituting (2.3.6) into (2.3.4).

$$\begin{aligned}\frac{d^2u(r(x))}{dr^2} &= \frac{1}{(r')^2}\Big[-\frac{r''}{r'}\big(C(r')^{C-1}r'' + (r')^C\frac{d}{dx}\big) \\ &+\big(C(C-1)(r')^{C-2}(r'')^2 + C(r')^{C-1}r''' + 2C(r')^{C-1}r''\frac{d}{dx} + (r')^C\frac{d^2}{dx^2}\big)\Big]f(x)\end{aligned} \tag{2.3.7}$$

Rearrange and bracket the first derivatives.

$$\begin{aligned}\frac{d^2u(r(x))}{dr^2} &= \frac{1}{(r')^2}\big[C(C-2)(r')^{C-2}(r'')^2 + C(r')^{C-1}r''' \\ &+ \big(2C(r')^{C-1}r'' - (r')^{C-1}r''\big)\frac{d}{dx} + (r')^C\frac{d^2}{dx^2}\big]f(x)\end{aligned} \tag{2.3.8}$$

Let the coefficient of the first derivative be zero

$$2C(r')^{C-1}r'' - (r')^{C-1}r'' = 0 \tag{2.3.9}$$

Calculate the C.

$$C = \frac{1}{2} \tag{2.3.10}$$

The exponent C is determined now.

With the given C, observe these terms without the first derivatives and second derivatives in (2.3.8).

$$\begin{aligned}&C(C-2)(r')^{C-2}(r'')^2 + C(r')^{C-1}r''' \\ =& -\frac{3}{4}(r')^{-\frac{3}{2}}(r'')^2 + \frac{1}{2}(r')^{-\frac{1}{2}}r'''\end{aligned} \tag{2.3.11}$$

$r(x)$ is given, and its derivatives, $r'(x)$, $r''(x)$, and $r'''(x)$, are easy to derive.

$$\begin{aligned}&C(C-2)(r')^{C-2}(r'')^2 + C(r')^{C-1}r''' \\ =& -\frac{3}{4}[\frac{(1-x+\alpha)^2}{2}]^{\frac{3}{2}}[\frac{4}{(1-x+\alpha)^3}]^2 + \frac{1}{2}[\frac{(1-x+\alpha)^2}{2}]^{\frac{1}{2}}\frac{12}{(1-x+\alpha)^4} \\ =& -\frac{3}{4}\frac{(1-x+\alpha)^3}{2\sqrt{2}}\frac{16}{(1-x+\alpha)^6} + \frac{1}{2}\frac{(1-x+\alpha)}{\sqrt{2}}\frac{12}{(1-x+\alpha)^4} \\ =& 0\end{aligned} \tag{2.3.12}$$

The given C also lets the summation be zero.

The variable change (2.3.6) with the given exponent C, $C = 1/2$, is

$$u(r(x)) = (r')^{\frac{1}{2}}f(x). \tag{2.3.13}$$

By the variable change (2.3.13), the second derivative of $u(r(x))$ with respect to r can be found from (2.3.8), (2.3.9), and (2.3.12) with the given C,

$$\frac{d^2u(r(x))}{dr^2} = \frac{1}{(r')^2}[0+0+(r')^{\frac{1}{2}}\frac{d^2}{dx^2}]f(x) = (r')^{-\frac{3}{2}}\frac{d^2f(x)}{dx^2}, \tag{2.3.14}$$

and the radial equation (2.3.2) becomes

$$-\frac{1}{2}(r')^{-\frac{3}{2}}\frac{d^2f(x)}{dx^2} + [\frac{l(l+1)}{2r^2} + V(r)](r')^{\frac{1}{2}}f(x) = E(r')^{\frac{1}{2}}f(x). \tag{2.3.15}$$

2.3.2 Construction and Symmetrization of Hamiltonian Matrix

The discretization of the differential operator by GPS and symmetrization of Hamiltonian matrix are introduced in this subsection.

Following paragraph describes how to apply GPS to the discretization of the differential operator. For the function $f(x)$ in (2.3.15), expand $f(x)$ in the cardinal functions $g_j(x)$ defined by (2.2.4),

$$f(x) = \sum_j g_j(x)f(x_j), \tag{2.3.16}$$

and the differential operator with respect to x works on the cardinal functions $g_j(x)$ but not $f(x_j)$.

$$\frac{d^2f(x)}{dx^2} = \sum_j \frac{d^2g(x)}{dx^2}f(x_j) \tag{2.3.17}$$

With (2.3.16) and (2.3.17), the radial equation (2.3.15) is on the pseudo-spectral basis.

$$\begin{aligned} &-\frac{1}{2}[r'(x_i)]^{-\frac{3}{2}}\sum_j \frac{d^2g_j(x)}{dx^2}f(x_j) + \big(\frac{l(l+1)}{2[r(x)]^2} + V(r(x))\big)[r'(x)]^{\frac{1}{2}}\sum_j g_j(x)f(x_j) \\ &= E\,[r'(x)]^{\frac{1}{2}}\sum_j g_j(x)f(x_j) \end{aligned} \tag{2.3.18}$$

Subsequently discretize x on GLL grids, $x = x_i$.

$$\begin{aligned} &-\frac{1}{2}[r'(x_i)]^{-\frac{3}{2}}\sum_j \frac{d^2g_j(x_i)}{dx^2}f(x_j) + \big(\frac{l(l+1)}{2[r(x_i)]^2} + V(r(x))\big)[r'(x_i)]^{\frac{1}{2}}\sum_j g_j(x_i)f(x_j) \\ &= E\,[r'(x_i)]^{\frac{1}{2}}\sum_j g_j(x_i)f(x_j) \end{aligned} \tag{2.3.19}$$

Both sides of (2.3.19) are divided by $[r'(x_i)]^{\frac{1}{2}}$, and take the summation notation and $f(x_j)$

out of the square brackets.

$$\sum_j \left[-\frac{1}{2}[r'(x_i)]^{-2}\frac{d^2 g_j(x_i)}{dx^2} + \Big(\frac{l(l+1)}{2[r(x_i)]^2} + V(r(x_i))\Big) g_j(x_i) \right] f(x_j) \\ = E \sum_j g_j(x_i) f(x_j) \tag{2.3.20}$$

The GPS has been performed, and whole equation is represented by discrete variables, x_i and x_j, in x domain.

In (2.3.20), the square bracket is a Hamiltonian matrix H. The H is non-symmetric due to the coefficient $[r'(x_i)]^{-2}$ of the second derivative. The non-symmetry leads to generalized eigenvalue problem of which eigenvalues and eigenfunction may have complex numbers. The rest in the subsection is to symmetrize the H to avoid the complex number occurring in solutions and speed up in solving the eigenvalue problem.

Substitute (2.2.3) and (2.2.33) into (2.3.20).

$$\sum_j \left[-\frac{1}{2}[r'(x_i)]^{-2} d''_{ij}\frac{P_N(x_i)}{P_N(x_j)} + \Big(\frac{l(l+1)}{2[r(x_i)]^2} + V(r(x_i))\Big)\delta_{ij} \right] f(x_j) \\ = E \sum_j \delta_{ij} f(x_j) \tag{2.3.21}$$

$f(x_j)$ multiplied by $r'(x_j)[P_N(x_j)]^{-1}$ becomes A_j.

$$\sum_j \left[-\frac{1}{2}[r'(x_i)]^{-2} d''_{ij}\frac{P_N(x_i)}{r'(x_j)} + \Big(\frac{l(l+1)}{2[r(x_i)]^2} + V(r(x_i))\Big)\delta_{ij}\frac{P_N(x_j)}{r'(x_j)} \right] A_j \\ = E \sum_j \delta_{ij}\frac{P_N(x_j)}{r'(x_j)} A_j \tag{2.3.22}$$

where

$$A_j = \frac{r'(x_j) f(x_j)}{P_N(x_j)}. \tag{2.3.23}$$

Because the property of δ_{ij}, let

$$\frac{P_N(x_j)}{r'(x_j)}\delta_{ij} = \frac{P_N(x_i)}{r'(x_i)}\delta_{ij}.$$

Eliminate the same coefficient, $P_N(x_i)[r'(x_i)]^{-1}$, on both sides.

$$\sum_j \left[-\frac{1}{2}[r'(x_i)]^{-1} d''_{ij}[r'(x_j)]^{-1} + \Big(\frac{l(l+1)}{2[r(x_i)]^2} + V(r(x_i))\Big)\delta_{ij} \right] A_j \\ = E \sum_j \delta_{ij} A_j \tag{2.3.24}$$

Because of δ_{ij}, the term, $i = j$, remains on the right side of the equation.

$$\sum_j \left[-\frac{1}{2}[r'(x_i)]^{-1} d''_{ij} [r'(x_j)]^{-1} + \Big(\frac{l(l+1)}{2[r(x_i)]^2} + V(r(x_i)) \Big) \delta_{ij} \right] A_j = \; E \; A_j \tag{2.3.25}$$

The terms in the square brackets form a *symmetric* Hamiltonian matrix H. The elements of the H are

$$H_{ij} = -\frac{1}{2}[r'(x_i)]^{-1} d''_{ij} [r'(x_j)]^{-1} + \Big(\frac{l(l+1)}{2[r(x_i)]^2} + V(r(x_i)) \Big) \delta_{ij}. \tag{2.3.26}$$

The centrifugal term and $V(r(x_i))$ only occur on the diagonal elements of the H. (2.3.25) is a *symmetric* eigenvalue problem. In physics, the Dirichlet boundary conditions,

$$A_0 = A_N = 0, \tag{2.3.27}$$

are usually used for the wave functions in quantum mechanics. We used the subset of GLL grids (2.1.9) that excludes the end points, $x_0 = -1$ and $x_N = 1$, to solve (2.3.25), and found the eigenvalues $\{E_n | n = 1, \ldots, N-1\}$ and the eigenstates $\{A_j | j = 1, \ldots, N-1\}$.

There are a brief of this section in Telnov and Chu (1999), and a similar work (Wang et al., 1994) that applies GPS to a Schrödinger equation.

2.3.3 Example: Hydrogen Atom

GPS with dense mesh is a good method to treat a system with the central potential. The dense mesh can effectively describe the variation near the point, $r = 0$, in the system. It lets the numerical calculation for the system by GPS be more accurate. For a example, we solved the Schrödinger Equation (SE) of a hydrogen atom that only has Coulomb potential.

The hydrogen atom is the simplest atomic problem. The single electron faces the bare Coulomb potential,

$$V(r) = -\frac{1}{4\pi\varepsilon_0}\frac{e^2}{r} \quad (SI) = -\frac{1}{r}, \tag{2.3.28}$$

of nucleus. From (2.3.1), the full SE of the electron with potential (2.3.28) under the assumption of infinite nucleus mass reads

$$[-\frac{1}{2}\nabla^2 - \frac{1}{r}]\psi(\mathbf{r}) = E\psi(\mathbf{r}) \tag{2.3.29}$$

The equation is analytically solvable. For bound states, the eigenvalues are

$$E_n(l) = -\frac{1}{2n^2} \quad n = l+1, l+2, \ldots, \tag{2.3.30}$$

and the eigenfunctions,

$$\psi(\mathbf{r}) = R_{n,l}(r)Y_{l,m}(\theta,\phi), \tag{2.3.31}$$

are composed of the radial and angular parts. The solutions of the angular part are spherical harmonics $Y_{l,m}(\theta,\phi)$, and the solutions of the radial part are

$$R_{n,l}(r) = N_{n,l}\exp(-\frac{r}{n})(\frac{2r}{n})^l L_{n-l-1}^{2l+1}(\frac{2r}{n}) \tag{2.3.32}$$

where $N_{n,l}$ is the normalization constant, and L_{n-l-1}^{2l+1} is associated Laguerre polynomials. (2.3.30) and (2.3.32) are the theoretical formulae to compare with numerical results.

For the numerical calculation, we suppose the angular part is given and only solve the radial equation (2.3.2) with the potential (2.3.28),

$$-\frac{1}{2}\frac{d^2}{dr^2}u(r) + [\frac{l(l+1)}{2r^2} - \frac{1}{r}]u(r) = Eu(r). \tag{2.3.33}$$

The radial equation of discretization is given by (2.3.25).

$$\sum_j \left[-\frac{1}{2}[r'(x_i)]^{-1}d''_{ij}[r'(x_j)]^{-1} + (\frac{l(l+1)}{2[r(x_i)]^2} - \frac{1}{r(x_i)}))\delta_{ij}\right] A_j = E\ A_j \tag{2.3.34}$$

In programming, the eigenvalue problem is solved by the library, LAPACK, built in the MKL (Math Kernel Library) which is developed and optimized by Intel. The numerical results are the eigenvalues and eigenfunctions. From the eigenfunctions, the radial functions are

$$R_{n,l}(r(x_j)) = \frac{A_j P_N(x_j)}{r(x_j)\sqrt{r'(x_j)}}. \tag{2.3.35}$$

Note that the $R_{n,l}(r(x_j))$ are not normalized yet.

We discretized r on 101 GLL grids that exclude end points, $x_0 = -1$ and $x_N = 1$, by the mapping function (2.1.15) with the length scale, $L = 10$. The maximum radius is $r_{max} = 100\,a.u.$.

With the 101×101 Hamiltonian matrix, 101 eigenvalues should be carried out. Table 2.3.1 gives the first 12 eigenvalues of (2.3.34) with angular quantum numbers, $l = 0 - 2$. On the 101 eigenvalues, only 8 eigenvalues are positive numbers, and the rest are negative numbers. The negative and positive eigenvalues are the bound and continuous states of hydrogen atom. The analysis formula of energy levels is only used for the the bound states, so the relative errors of continuous states and exact values are denoted the abbreviation of "not applicable".

Table 2.3.1: Energy levels of neutral hydrogen atom from the solution of radial equation with angular quantum numbers, $l = 0 - 2$, by GPS method.

n	Numerical $E_n(l)$						Exact
	$l = 0$	RE[a]	$l = 1$	RE[a]	$l = 2$	RE[a]	
1	−5.0000[−01]	4.1078[−15]					−5.0000[−01]
2	−1.2500[−01]	1.9762[−14]	−1.2500[−01]	1.4655[−14]			−1.2500[−01]
3	−5.5556[−02]	1.6986[−14]	−5.5556[−02]	2.4855[−14]	−5.5556[−02]	4.2466[−15]	−5.5556[−02]
4	−3.1250[−02]	1.2858[−11]	−3.1250[−02]	8.4733[−12]	−3.1250[−02]	3.4517[−12]	−3.1250[−02]
5	−2.0000[−02]	1.4248[−06]	−2.0000[−02]	1.0685[−06]	−2.0000[−02]	5.7910[−07]	−2.0000[−02]
6	−1.3868[−02]	1.4696[−03]	−1.3872[−02]	1.2291[−03]	−1.3877[−02]	8.4172[−04]	−1.3889[−02]
7	−9.5964[−03]	5.9555[−02]	−9.6532[−03]	5.3990[−02]	−9.7560[−03]	4.3917[−02]	−1.0204[−02]
8	−4.6628[−03]	4.0316[−01]	−4.8446[−03]	3.7989[−01]	−5.1876[−03]	3.3599[−01]	−7.8125[−03]
9	1.6561[−03]	n/a	1.3231[−03]	n/a	6.92438[−04]	n/a	−6.1728[−03]
10	9.2667[−03]	n/a	8.7639[−03]	n/a	7.81785[−03]	n/a	−5.0000[−03]
11	1.8084[−02]	n/a	1.7393[−02]	n/a	1.61070[−02]	n/a	−4.1322[−03]
12	2.8055[−02]	n/a	2.7159[−02]	n/a	2.55118[−02]	n/a	−3.4722[−03]

[a] 'RE' is the abbreviation of 'relative error' of numerical and exact value.

For the various angular quantum number, $l = 0-2$, as listed in Table 2.3.1, the energy levels n start from $l + 1$. It matches the relation, $l = 0, 1, \ldots, n - 1$, of angular quantum number l and principal quantum number n in theory.

The smallest order of magnitude for the bound and continuous states is about -3 as indicated in tables 2.3.1. Under the conditions, the smallest order is the limit of the numerical calculation by GPS. The bound states are dense when the states are close to the boundary. On the finite pseudo-spectral basis and grids, it is hard to numerically calculate the dense states near the boundary, $E = 0$, by GPS and thus leads to the limit.

From Table 2.3.1, the maximum number of bound states which can be evaluated by GPS always occurs when $l = 0$. The l is increasing by 1, and the number of bound states is decreasing by 1 or not changed. the number of bound states may have one at least.

The eigenfunctions corresponding to the eigenvalues are plotted in Figure 2.3.1. The dot, dash, and solid lines are the exactly wave functions of $n = 1$, $n = 2$, and $n = 3$ with various l. The discrete points, plotted by circles, crosses, x marks, squares, triangles, and rhombuses, are the wave functions numerically calculated by GPS.

Figure 2.3.1: Radial function of a neutral hydrogen atom evaluated by GPS and theoretical formulae. The line is exact, and the points are numerical results.

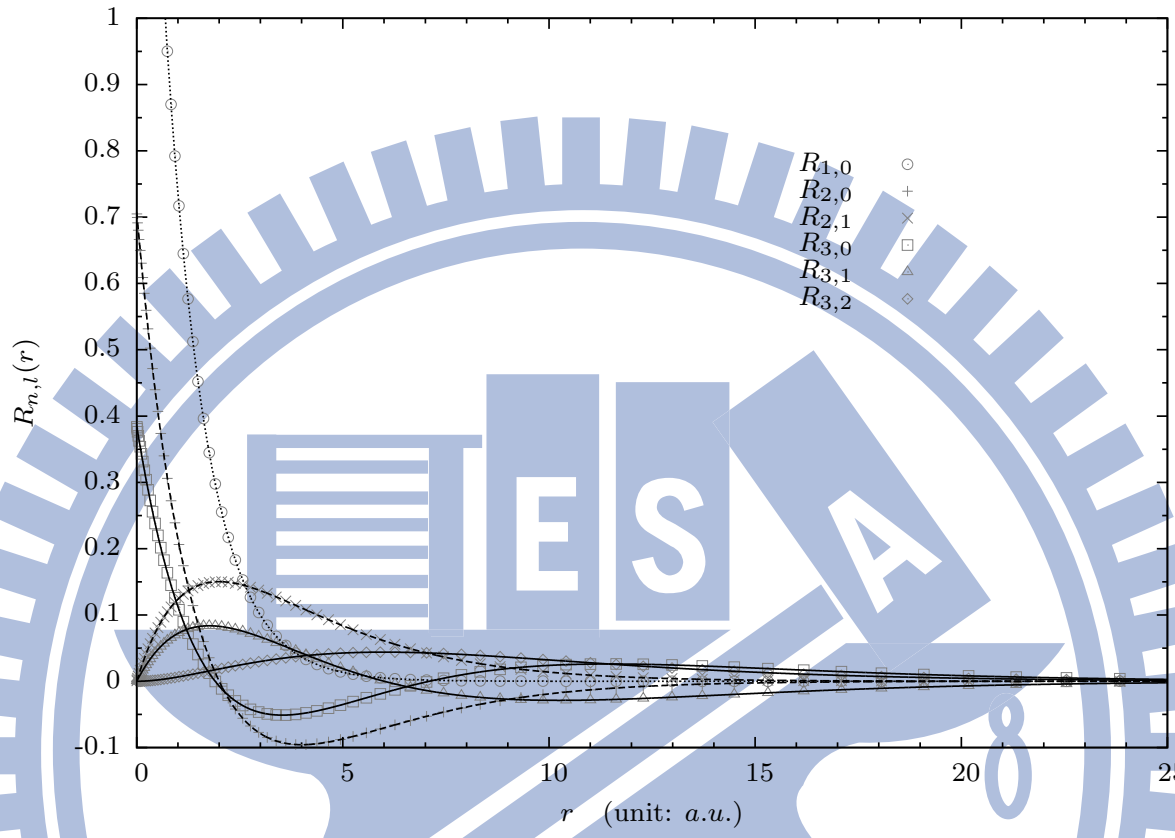

Figure 2.3.1 only displays the wave functions where $r < 25\,a.u.$ because they all rapidly decay to zero. The oscillations of wave functions mostly occur near the original point, $r = 0$. The wave functions fully utilize the feature of dense mesh.

2.4 Application of GPS on Poisson's Equation

The Hartree potential $V_H(\mathbf{r})$ is a model that approximate the electrostatic interaction of a electron due to all the other electrons in a system. The model assumes that the summation of state of individual electron is straightforward to construct the charge density distribution $\rho(\mathbf{r})$. By integration of $\rho(\mathbf{r})$ over all space, the $V_H(\mathbf{r})$ is

$$V_H(\mathbf{r}) = \int \frac{\rho(\mathbf{r}')}{|\mathbf{r}-\mathbf{r}'|} d\mathbf{r}'. \tag{2.4.1}$$

It is not easy to directly calculate the integration due to the $|\mathbf{r}-\mathbf{r}'|^{-1}$, so the other method to calculate the $V_H(\mathbf{r})$ is necessary. The $V_H(\mathbf{r})$ satisfies the Poisson's equation by Gauss law.

$$\nabla^2 V_H(\mathbf{r}) = -4\pi\rho(\mathbf{r}) \tag{2.4.2}$$

Through solving the Poisson's equation, the $V_H(\mathbf{r})$ can be found.

The second application of GPS is a solver for Poisson's equation. The main body of this section is the discretization of the derivatives by GPS and construction of the the system equation. The boundary conditions can correct the solver, and make the calculation more accurate. The end of this section is a example.

2.4.1 Separation of Radial Part from Poisson's Equation

The Poisson's equation in atomic unit reads

$$\nabla^2 V(\mathbf{r}) = -4\pi\rho(\mathbf{r}) \tag{2.4.3}$$

where $V(\mathbf{r})$ is the potential due to the source $\rho(\mathbf{r})$, and $\rho(\mathbf{r})$ is the electric charge distribution. Expand both $V(\mathbf{r})$ and $\rho(\mathbf{r})$ in spherical harmonics $Y_{l,m}(\theta,\phi)$.

$$V(\mathbf{r}) = \sum_l \sum_m V_{l,m}(r) Y_{l,m}(\theta,\phi) \tag{2.4.4}$$

$$\rho(\mathbf{r}) = \sum_l \sum_m \rho_{l,m}(r) Y_{l,m}(\theta,\phi) \tag{2.4.5}$$

Assume that $\rho(\mathbf{r})$ is azimuthal symmetry. The $\rho(\mathbf{r})$ is independent of ϕ, and let $m = 0$ in the expansion.

$$V(\mathbf{r}) = \sum_l V_l(r) Y_{l,0}(\theta,\phi) = \sum_l \frac{u_l(r)}{r} Y_{l,0}(\theta,\phi) \tag{2.4.6}$$

$$\rho(\mathbf{r}) = \sum_l \rho_l(r) Y_{l,0}(\theta,\phi) \tag{2.4.7}$$

Substitute the expansions of $V(\mathbf{r})$ and $\rho(\mathbf{r})$, (2.4.7) and (2.4.6), into Poisson's equation (2.4.3).

$$\sum_l \nabla^2 \left[\frac{u_l(r)}{r} Y_{l,0}(\theta,\phi) \right] = -4\pi \sum_l \rho_l(r) Y_{l,0}(\theta,\phi) \tag{2.4.8}$$

Because

$$Y_{l,0}(\theta,\phi) = \sqrt{\frac{2l+1}{4\pi}} P_l(x) \tag{2.4.9}$$

where $x = \cos\theta$, the differential operators with respect to ϕ have no work, and (2.4.8) becomes

$$\begin{aligned} &\sum_l \left[Y_{l,0}(\theta,\phi) \frac{1}{r^2} \frac{d}{dr} \Big(r^2 \frac{d}{dr} \big(\frac{u_l(r)}{r} \big) \Big) + \big(\frac{u_l(r)}{r} \big) \frac{1}{r^2 \sin\theta} \frac{d}{d\theta} \Big(\sin\theta \frac{dY_{l,0}(\theta,\phi)}{d\theta} \Big) \right] \\ &= -4\pi \sum_l \rho_l(r) Y_{l,0}(\theta,\phi) \end{aligned} \tag{2.4.10}$$

$Y_{l,0}(\theta,\phi)$ are the eigenfunctions of the angular momentum operator L^2, so the angular momentum operator L^2, which works on its eigenfunctions $Y_{l,0}(\theta,\phi)$, can be replaced by its eigenvalue $-l(l+1)$.

$$\sum_l \left[\frac{Y_{l,0}(\theta,\phi)}{r} \frac{d^2 u_l(r)}{dr^2} - \big(\frac{u_l(r)}{r} \big) \frac{l(l+1)}{r^2} Y_{l,0}(\theta,\phi) \right] = -4\pi \sum_l \rho_l(r) Y_{l,0}(\theta,\phi) \tag{2.4.11}$$

Take $Y_{l,0}(\theta,\phi)$ out of the square brackets, and multiply r to both sides.

$$\sum_l \left[\frac{d^2 u_l(r)}{dr^2} - \frac{l(l+1)}{r^2} u_l(r) \right] Y_{l,0}(\theta,\phi) = -4\pi r \sum_l \rho_l(r) Y_{l,0}(\theta,\phi) \tag{2.4.12}$$

The coefficients of $Y_{l,0}(\theta,\phi)$ provide

$$\frac{d^2 u_l(r)}{dr^2} - \frac{l(l+1)}{r^2} u_l(r) = -4\pi r \rho_l(r) \tag{2.4.13}$$

(2.4.13) is one of partially radial equations.

2.4.2 Construction of System of Linear Equations

Remaining steps are the discretization of the partially radial equation (2.4.13). Apply variable change, (2.3.13) and (2.3.14), to (2.4.13).

$$[r'(x)]^{-\frac{3}{2}} \frac{d^2 f_l(x)}{dx^2} - \frac{l(l+1)}{r^2} [r'(x)]^{\frac{1}{2}} f_l(x) = -4\pi r \rho_l(r) \tag{2.4.14}$$

This equation is mapped to x domain. Multiply $[r'(x)]^{3/2}$ to both sides of (2.4.14), and the coefficient of $f_l''(x)$ becomes unity,

$$\frac{d^2 f_l(x)}{dx^2} - l(l+1) \big(\frac{r'(x)}{r(x)} \big)^2 f_l(x) = -4\pi r(x) [r'(x)]^{\frac{3}{2}} \rho_l(r). \tag{2.4.15}$$

Apply GPS to discretize the $f_l(x)$ on the pseudo-spectral basis. Expand $f_l(x)$ in the cardinal functions (2.2.4).

$$\sum_j \left[\frac{d^2 g_j(x)}{dx^2} - l(l+1)(\frac{r'(x)}{r(x)})^2 g_j(x)\right] f_l(x_j) = -4\pi r(x)[r'(x)]^{\frac{3}{2}}\rho_l(r) \tag{2.4.16}$$

Discretize x on GLL grid, $x = x_i$.

$$\sum_j \left[\frac{d^2 g_j(x_i)}{dx^2} - l(l+1)(\frac{r'(x_i)}{r(x_i)})^2 g_j(x_i)\right] f_l(x_j) = -4\pi r(x_i)[r'(x_i)]^{\frac{3}{2}}\rho_l(r(x_i)) \tag{2.4.17}$$

$g_j''(x_i)$ and $g_j(x_i)$ are given by (2.2.24) and (2.2.33).

$$\sum_j \left[d''_{ij}\frac{P_N(x_i)}{P_N(x_j)} - l(l+1)(\frac{r'(x_i)}{r(x_i)})^2\delta_{ij}\right] f_l(x_j) = -4\pi r(x_i)[r'(x_i)]^{\frac{3}{2}}\rho_l(r(x_i)) \tag{2.4.18}$$

Inserting $P_N(x_i)[P_N(x_j)]^{-1}$ to δ_{ij} as a coefficient does not affect this equation because of the property of δ_{ij}.

$$\sum_j \left[d''_{ij}\frac{P_N(x_i)}{P_N(x_j)} - l(l+1)(\frac{r'(x_i)}{r(x_i)})^2\delta_{ij}\frac{P_N(x_i)}{P_N(x_j)}\right] f_l(x_j) = -4\pi r(x_i)(r'(x_i))^{\frac{3}{2}}\rho_l(r(x_i)) \tag{2.4.19}$$

Take $[P_N(x_j)]^{-1}$ out the square brackets, and eliminate $P_N(x_i)$ on both sides.

$$\sum_j \left[d''_{ij} - l(l+1)(\frac{r'(x_i)}{r(x_i)})^2\delta_{ij}\right]\frac{f_l(x_j)}{P_N(x_j)} = -4\pi r(x_i)[r'(x_i)]^{\frac{3}{2}}\frac{\rho_l(r(x_i))}{P_N(x_i)} \tag{2.4.20}$$

With all GLL grids $\{x_i | i = 0, 1, \cdots, N\}$, the partially radial equations form a system of linear equations,

$$\begin{bmatrix} D_{0,0} & D_{0,1} & \cdots & D_{0,N-1} & D_{0,N} \\ D_{1,0} & D_{1,1} & \cdots & D_{0,N-1} & D_{1,N} \\ \vdots & \vdots & \ddots & \vdots & \vdots \\ D_{N-1,0} & D_{N-1,1} & \cdots & D_{N-1,N-1} & D_{N-1,N} \\ D_{N,0} & D_{N,1} & \cdots & D_{N,N} & D_{N,N} \end{bmatrix} \begin{bmatrix} a_0 \\ a_1 \\ \vdots \\ a_{N-1} \\ a_N \end{bmatrix} = \begin{bmatrix} b_0 \\ b_1 \\ \vdots \\ b_{N-1} \\ b_N \end{bmatrix} \tag{2.4.21}$$

where

$$D_{ij} = d''_{ij} - l(l+1)(\frac{r'(x_i)}{r(x_i)})^2\delta_{ij}, \tag{2.4.22}$$

$$a_j = \frac{f_l(x_j)}{P_N(x_j)}, \tag{2.4.23}$$

$$b_i = -4\pi r(x_i)[r'(x_i)]^{\frac{3}{2}}\frac{\rho_l(r(x_i))}{P_N(x_i)}. \tag{2.4.24}$$

If all a_j are carried out directly from the linear system (2.4.21) without any correction, the inaccuracy is unavoidable because boundary the conditions, a_0 and a_N, are unknown. The boundary conditions can be numerically calculated by Gaussian quadrature.

2.4.3 Determination of Boundary Conditions

This subsection represents the numerical calculation of the boundary conditions by Gaussian quadrature.

When the electric charge distribution $\rho(\mathbf{r})$ is given, the potential can be calculated by the integration over all space,

$$V(\mathbf{r}) = \int \frac{\rho(\mathbf{r}')}{|\mathbf{r}-\mathbf{r}'|} d^3\mathbf{r}'. \tag{2.4.25}$$

The expansion of $V(\mathbf{r})$ and $\rho(\mathbf{r})$ in spherical harmonics are given by (2.4.6) and (2.4.7).

$$\sum_{l'} \frac{u_{l'}(r)}{r} Y_{l',0}(\theta,\phi) = \sum_{l'} \int \frac{\rho_{l'}(r') Y_{l',0}(\theta',\phi')}{|\mathbf{r}-\mathbf{r}'|} d^3\mathbf{r}' \tag{2.4.26}$$

The fraction $|\mathbf{r}-\mathbf{r}'|^{-1}$ can also be expanded in the spherical harmonic functional space.

$$\frac{1}{|\mathbf{r}-\mathbf{r}'|} = \sum_l \sum_m \frac{4\pi}{2l+1} \frac{r_<^l}{r_>^{l+1}} Y_{l,m}^*(\theta',\phi') Y_{l,m}(\theta,\phi) \tag{2.4.27}$$

With the expansion of $|\mathbf{r}-\mathbf{r}'|^{-1}$, (2.4.26) becomes

$$\begin{aligned} &\sum_{l'} \frac{u_{l'}(r)}{r} Y_{l',0}(\theta,\phi) \\ &= \sum_{l',l,m} \frac{4\pi}{2l+1} Y_{l,m}(\theta,\phi) \int \frac{r_<^l}{r_>^{l+1}} \rho_l(r') r'^2 dr' \int Y_{l,m}^*(\theta',\phi') Y_{l',0}(\theta',\phi') d\Omega' \end{aligned} \tag{2.4.28}$$

The integration of the production of two spherical harmonics is analysis by the orthogonality of spherical harmonics,

$$\int Y_{l,m}^*(\theta,\phi) Y_{l',0}(\theta,\phi) d\Omega = \delta_{l,l'}\delta_{m,0} \tag{2.4.29}$$

Because of the property of Kronecker delta δ_{ij}, the terms only with $l' = l$ and $m = 0$ remain in (2.4.28).

$$\sum_l \frac{u_l(r)}{r} Y_{l,0}(\theta,\phi) = \sum_l \frac{4\pi}{2l+1} \int \frac{r_<^l}{r_>^{l+1}} \rho_l(r') r'^2 dr' Y_{l,0}(\theta,\phi) \tag{2.4.30}$$

The coefficients of $Y_{l,0}(\theta,\phi)$ provide

$$\frac{u_l(r)}{r} = \frac{4\pi}{2l+1} \int \frac{r_<^l}{r_>^{l+1}} \rho_l(r') r'^2 dr \tag{2.4.31}$$

The infinite interval $[0,\infty]$ is limited to the finite interval $[r_{min}, r_{max}]$ on the Gaussian grids by the mapping function. Split the finite interval, $[r_{min}, r_{max}]$, into two subintervals,

$[r_{min}, r]$ and $[r, r_{max}]$. $r_>$ and $r_<$ are determined in individual subinterval. In the subinterval, $[r_{min}, r]$, $r_>$ and $r_<$ are r and r'. In the other subinterval, $[r, r_{max}]$, $r_>$ and $r_<$ are r' and r.

$$\frac{u_l(r)}{r} = \frac{4\pi}{2l+1}[\int_{r_{min}}^{r} \frac{r'^l}{r^{l+1}}\rho_l(r')r'^2dr' + \int_{r}^{r_{max}} \frac{r^l}{r'^{l+1}}\rho_l(r')r'^2dr'] \tag{2.4.32}$$

Rearrange the equation.

$$u_l(r) = \frac{4\pi}{2l+1}[\frac{1}{r^l}\int_{r_{min}}^{r} r'^l\rho_l(r')r'^2dr' + r^{l+1}\int_{r}^{r_{max}} \frac{\rho_l(r')}{r'^{l-1}}dr'] \tag{2.4.33}$$

At the first point, $r = r_{min}$, $u_l(r_{min})$ is one of two boundary conditions,

$$u_l(r_{min}) = \frac{4\pi}{2l+1}[\frac{1}{r_{min}^l}\int_{r_{min}}^{r_{min}} r'^l\rho_l(r')r'^2dr' + r_{min}^{l+1}\int_{r_{min}}^{r_{max}} \frac{\rho_l(r')}{r'^{l-1}}dr']. \tag{2.4.34}$$

According to the definition of calculus, the first integration is zero, so

$$u_l(r_{min}) = \frac{4\pi r_{min}^{l+1}}{2l+1}\int_{r_{min}}^{r_{max}} \frac{\rho_l(r')}{r'^{l-1}}dr'. \tag{2.4.35}$$

At the last point r_{max}, $u(r_{max})$ is the other one of two boundary conditions,

$$u_l(r_{max}) = \frac{4\pi}{2l+1}[\frac{1}{r_{max}^l}\int_{r_{min}}^{r_{max}} r'^l\rho_l(r')r'^2dr' + r_{max}^{l+1}\int_{r_{max}}^{r_{max}} \frac{\rho_l(r')}{r'^{l-1}}dr']. \tag{2.4.36}$$

By the same way, the second integration is zero, so

$$u_l(r_{max}) = \frac{4\pi}{(2l+1)r_{max}^l}\int_{r_{min}}^{r_{max}} r'^{l+2}\rho_l(r')dr'. \tag{2.4.37}$$

Discretize $u_l(r)$ on the GLL grids by the mapping function (2.1.15). r_{min} and r_{max} are r_0 and r_N given by (2.1.16) and (2.1.17). After $u_l(r_0)$ and $u_l(r_N)$ are calculated by the equations, (2.4.35) and (2.4.37), a_0 and a_N can be calculated by the relations, (2.3.13) and (2.4.23). Actually, $u_l(r_{min})$ can be ignored because $r_{min} = r_0 = 0$ in (2.4.35).

2.4.4 Correction to Solver

With the given boundary conditions, a_0 and a_N, correct and simplify (2.4.21) in this subsection.

the a_0 and a_N do not need to be calculated from the system of linear equations again. The first and last equations (in bold font) in (2.4.21) are for the a_0 and a_N.

$$\begin{bmatrix} \mathbf{D_{0,0}} & \mathbf{D_{0,1}} & \cdots & \mathbf{D_{0,N-1}} & \mathbf{D_{0,N}} \\ D_{1,0} & D_{1,1} & \cdots & D_{1,N-1} & D_{1,N} \\ \vdots & \vdots & \ddots & \vdots & \vdots \\ D_{N-1,0} & D_{N-1,1} & \cdots & D_{N-1,N-1} & D_{N-1,N} \\ \mathbf{D_{N,0}} & \mathbf{D_{N,1}} & \cdots & \mathbf{D_{N,N-1}} & \mathbf{D_{N,N}} \end{bmatrix} \begin{bmatrix} \mathbf{a_0} \\ a_1 \\ \vdots \\ a_{N-1} \\ \mathbf{a_N} \end{bmatrix} = \begin{bmatrix} \mathbf{b_0} \\ b_1 \\ \vdots \\ b_{N-1} \\ \mathbf{b_N} \end{bmatrix} \tag{2.4.38}$$

Remove the first and last equations (in bold font) in (2.4.38), and the dimensions of matrix and vector are reduced to $N-1 \times N-1$ and $N-1$.

$$\begin{bmatrix} D_{1,1} & \cdots & D_{1,N-1} \\ \vdots & \ddots & \vdots \\ D_{N-1,1} & \cdots & D_{N-1,N-1} \end{bmatrix} \begin{bmatrix} a_1 \\ \vdots \\ a_{N-1} \end{bmatrix} = \begin{bmatrix} b_1 \\ \vdots \\ b_{N-1} \end{bmatrix} \tag{2.4.39}$$

Treat these terms,

$$\{D_{i,0}a_0 | i = 1, \cdots, N-1\}$$

and

$$\{D_{i,N}a_N | i = 1, \cdots, N-1\},$$

involving a_0 and a_N in the matrix-vector product in (2.4.38) as *correction terms*. Add these correction terms, $D_{i,0}a_0$ and $D_{i,N}a_N$, as two column vectors back to the matrix-vector product.

$$\begin{bmatrix} D_{1,1} & \cdots & D_{1,N-1} \\ \vdots & \ddots & \vdots \\ D_{N-1,1} & \cdots & D_{N-1,N-1} \end{bmatrix} \begin{bmatrix} a_1 \\ \vdots \\ a_{N-1} \end{bmatrix} + \begin{bmatrix} D_{1,0}a_0 \\ \vdots \\ D_{N-1,0}a_0 \end{bmatrix} + \begin{bmatrix} D_{1,N}a_N \\ \vdots \\ D_{N-1,N}a_N \end{bmatrix} = \begin{bmatrix} b_1 \\ \vdots \\ b_{N-1} \end{bmatrix} \tag{2.4.40}$$

The a_0 is zero because $r(x_0) = 0$ on GLL grids, so the column vector $D_{i,0}a_0$ is a zero vector. Move the column vector $D_{i,N}a_N$ to the other side.

$$\begin{bmatrix} D_{1,1} & \cdots & D_{1,N-1} \\ \vdots & \ddots & \vdots \\ D_{N-1,1} & \cdots & D_{N-1,N-1} \end{bmatrix} \begin{bmatrix} a_1 \\ \vdots \\ a_{N-1} \end{bmatrix} = \begin{bmatrix} b_1 \\ \vdots \\ b_{N-1} \end{bmatrix} - \begin{bmatrix} D_{1,N}a_N \\ \vdots \\ D_{N-1,N}a_N \end{bmatrix} \tag{2.4.41}$$

where the D_{ij}, a_j, and b_i are the same as (2.4.22), (2.4.23), and (2.4.24), but the lower and upper bound of both indexes, i and j, become 1 and $N-1$.

Numerically solve the system of linear equations, and find $\{a_j | j = 1, \cdots, N-1\}$. One of $u_l(r)$ is numerically calculated through (2.4.23) and (2.3.13). With the various l, all $u_l(r)$ are solved. The potential $V(\mathbf{r})$ is the summation of $u_l(r)$ by (2.4.4).

Many articles may not indicate how to calculate the Hartree potential. Jiang et al. (2001) have a brief about the extension of GPS to solve the Poisson's equation.

2.4.5 Example: Potential Due to Square of Eigenstate

For a example, treat square of the eigenstate $\Psi_{210}(\mathbf{r})$ of a hydrogen atom as a source $\rho(\mathbf{r})$,

$$\rho(\mathbf{r}) = |R_{12}(r)|^2 Y_{1,0}^*(\theta,\phi) Y_{1,0}(\theta,\phi) = \frac{r^2}{24} e^{-r} Y_{1,0}^*(\theta,\phi) Y_{1,0}(\theta,\phi), \tag{2.4.42}$$

and solve the Poisson's equation due to this resource $\rho(\mathbf{r})$ by GPS.

The components of $\rho(\mathbf{r})$ in spherical harmonics $Y_{1,0}(\theta,\phi)$ are

$$\rho_0(r) = \sqrt{\frac{1}{4\pi}} |R_{12}(r)|^2 \tag{2.4.43}$$

and,

$$\rho_2(r) = \sqrt{\frac{3}{15\pi}} |R_{12}(r)|^2. \tag{2.4.44}$$

All other components are zero.

The components of potential $V_l(r)$ corresponding to $\rho_0(r)$ and ρ_2 are

$$V_0(r) = \frac{\sqrt{\pi}}{12} r^{-1} [24 - (r^3 + 6r^2 + 18r + 24) e^{-r}] \tag{2.4.45}$$

and,

$$V_2(r) = \frac{\sqrt{\pi}}{6\sqrt{5}} r^{-3} [144 - (r^5 + 6r^4 + 24r^3 + 72r^2 + 144r + 144) e^{-r}] \tag{2.4.46}$$

in theory. As same as $\rho_l(r)$, all other components are zero.

We numerically solved the Poisson's equations by method 1 and method 2. The method 1 is the direct solution of the linear system (2.4.21) *without* the boundary conditions only on the subset of GLL grids, $\{x_i | i = 1, \cdots, N-1\}$, to avoid diverging at the end point, $r = 0$. The method 2 is that perform the calculations of the boundary conditions first, and solve the linear system (2.4.41) *with* the given boundary conditions on the subset of GLL grids, $\{x_i | i = 1, \cdots, N-1\}$.

the relative errors on the first 10 grids and the last 10 grids are listed in Table 2.4.1. All relative errors are plotted in Figure 2.4.1 versus the index i of GLL grid. In Figure 2.4.1, the method 1 is dash line, and the method 2 is solid line. The relative error at the end point, $r = r_{max}$, is only listed in Table 2.4.1. There were 203 GLL grids used in the numerical calculation, and discretized r domain, $[0, 200]$, on the subset of GLL grids by the mapping function (2.1.15) with length scale, $L = 20$.

Table 2.4.1: Relative errors of Hatree potential at the points near the boundaries from the numerical solution of Poisson's equation by GPS.

i	r_i	method 1		method 2		exact	
		$l=0$	$l=2$	$l=0$	$l=2$	$l=0$	$l=2$
1	0.00	2.04[−02]	1.14[+01]	1.09[−12]	1.14[+01]	8.86[−01]	8.71[−07]
2	0.01	2.04[−02]	1.29[−03]	3.80[−13]	1.29[−03]	8.86[−01]	7.86[−07]
3	0.01	2.04[−02]	1.16[−04]	4.55[−14]	1.16[−04]	8.86[−01]	3.48[−06]
4	0.02	2.04[−02]	3.66[−05]	7.37[−14]	3.66[−05]	8.86[−01]	1.02[−05]
5	0.03	2.04[−02]	1.15[−06]	1.76[−13]	1.15[−06]	8.86[−01]	2.39[−05]
6	0.04	2.04[−02]	7.21[−08]	2.35[−13]	6.99[−08]	8.86[−01]	4.82[−05]
7	0.06	2.04[−02]	2.58[−08]	3.78[−13]	2.80[−08]	8.86[−01]	8.73[−05]
8	0.07	2.04[−02]	3.43[−08]	4.03[−13]	3.66[−08]	8.86[−01]	1.47[−04]
9	0.09	2.04[−02]	9.83[−09]	3.37[−13]	1.21[−08]	8.86[−01]	2.32[−04]
10	0.12	2.04[−02]	4.36[−09]	2.24[−13]	2.10[−09]	8.86[−01]	3.50[−04]
...	.....	.....	.....	.....	.....	....	....
192	186.95	1.43[+01]	2.49[+00]	7.64[−13]	5.43[−13]	1.90[−02]	2.91[−06]
193	189.25	1.76[+01]	3.14[+00]	8.14[−13]	6.31[−13]	1.87[−02]	2.81[−06]
194	191.37	2.22[+01]	4.05[+00]	7.82[−13]	6.40[−13]	1.85[−02]	2.71[−06]
195	193.27	2.87[+01]	5.36[+00]	6.65[−13]	5.57[−13]	1.83[−02]	2.64[−06]
196	194.96	3.87[+01]	7.35[+00]	4.90[−13]	4.09[−13]	1.82[−02]	2.57[−06]
197	196.42	5.49[+01]	1.06[+01]	4.67[−13]	4.06[−13]	1.80[−02]	2.51[−06]
198	197.65	8.39[+01]	1.64[+01]	4.10[−13]	3.69[−13]	1.79[−02]	2.46[−06]
199	198.62	1.44[+02]	2.84[+01]	5.65[−13]	5.38[−13]	1.78[−02]	2.43[−06]
200	199.34	3.03[+02]	6.02[+01]	8.61[−13]	8.50[−13]	1.78[−02]	2.40[−06]
201	199.80	1.02[+03]	2.03[+02]	4.51[−13]	4.50[−13]	1.77[−02]	2.39[−06]
202	200.00	n/a	n/a	1.96[−16]	0.00[+00]	1.77[−02]	2.38[−06]

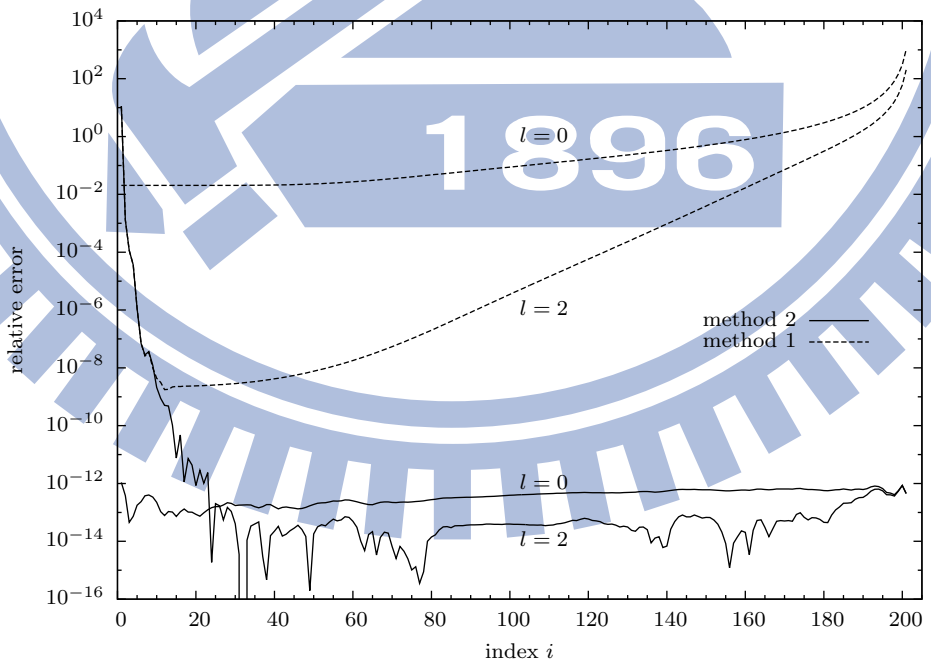

Figure 2.4.1: Logarithm of relatives errors of Hatree potential from the numerical solution of Poisson's equation by GPS.

The maximum relative error can be found in Figure 2.4.1. The maximum relative error occurs at the points, r_1 or r_{N-1}, close to the boundary. Not surprisingly, it is a feature of GPS.

The $V_0(r)$ by method 1 only has about 1 significant figure behind the decimal point over all grids. The $V_2(r)$ by method 1 has better accuracy, but it can not rescue the accuracy of total potential $V(\mathbf{r})$ because the $V_2(r)$ is far less than the $V_0(r)$. The method 1 is not reliable mainly due to the few significant figures.

On the other hand, the $V_0(r)$ by method 2 has over 10 significant figures behind the decimal point over all grids as listed in Table 2.4.1. At the first point, the relative errors of $V_2(r)$ by method 2 have the same order of magnitude as $V_2(r)$ by method 1. The $V_2(r)$ has about 5 significant figures behind the decimal point. When sum all components, the $V(\mathbf{r})$ only has 5 significant figures behind the decimal point. The method 2 is better than the method 1 on the whole. The correction terms has apparent effect on the numerical calculation and lead to better accuracy.

If the numerical calculation needs to avoid the inaccuracy at the points near the boundary, $r = 0$, increase in the length scale L of the mapping function (2.1.15) is a possible ways. The increase in L can change the distribution of $r(x_i)$, and let the first point $r(x_1)$ be located the point, $r > 0.1$ by the mapping function (2.1.15). As shown in Table 2.4.1, the relative errors of $V_2(r)$ by method 2 on the grids, $r > 0.1$, are less than 10^{-8}. It can decrease the maximum relative error over all grids because $V_2(r)$ by method 2 dominate the accuracy in method 2.

2.5 Split Operator Method

The state functions of system vary with time when the system is under a time-dependent field. To carry out these state functions, it requires a method to deal with the time variable of time-dependent equation. We chose the split operator method to split the total Hamiltonian operator. This section provides the introduction to split operator method, calculation of operator, and the process in programming.

2.5.1 Intorduction

The time-independent Schrödinger equation (SE) by GPS gives the stationary states. Treat the stationary states as a initial value, and the time-dependent Schrödinger equation (TDSE) becomes a initial value problem. This split operator method is widely employed to numerically solve the initial value problem.

Consider following differential equation with the initial condition $u(t=0)$.

$$\frac{d}{dt}u(t) = \hat{A}u(t) \tag{2.5.1}$$

where $\hat{A}$ is a sum of two operators, $\hat{A}_1$ and $\hat{A}_2$, which do not commute.

Discretize time t by the time length Δt. In a subinterval $[t, t+\Delta t]$, the true solution for the equation (2.5.1) is

$$u(t+\Delta t) = e^{(\hat{A}_1+\hat{A}_2)\Delta t}u(t) \tag{2.5.2}$$

The simplest approximations is divide and rule. Treat the one of operators first and the other later.

$$u(t+\Delta t) \approx e^{\hat{A}_1\Delta t}e^{\hat{A}_2\Delta t}u(t), \tag{2.5.3}$$

or vice versa

$$u(t+\Delta t) \approx e^{\hat{A}_2\Delta t}e^{\hat{A}_1\Delta t}u(t). \tag{2.5.4}$$

The operator $\hat{A}$ is *split* into $\hat{A}_1$ and $\hat{A}_2$ for the approximation. The splitting forms, (2.5.3) and (2.5.4), are called **Lie splitting** proposed by Trotter (1959).

The local truncation error of Lie splitting can be found by the Baker-Campbell-Hausdorff formula. After a time step Δt, the Lie splitting give rise to the local truncation error of

$$\frac{\Delta t^2}{2}[\hat{A}_1, \hat{A}_2]u(t) + O(\Delta t^3) \tag{2.5.5}$$

where $[\hat{A}_1, \hat{A}_2]$ is the commutator of $\hat{A}_1$ and $\hat{A}_2$. The local truncation error (2.5.5) has no Δt term, so the Lie splitting is accurate in the first order.

The leading term in the local truncation error of Lie splitting is the antisymmetry of $\hat{A}_1$ and $\hat{A}_2$. The observation on the antisymmetry leads to a symmetric splitting form,

$$u(t+\Delta t) \approx e^{\hat{A}_1 \frac{\Delta t}{2}} e^{\hat{A}_2 \frac{\Delta t}{2}} (e^{\hat{A}_2 \frac{\Delta t}{2}} e^{\hat{A}_1 \frac{\Delta t}{2}} u(t)) = e^{\hat{A}_1 \frac{\Delta t}{2}} e^{\hat{A}_2 \Delta t} e^{\hat{A}_1 \frac{\Delta t}{2}} u(t), \tag{2.5.6}$$

or vice versa

$$u(t+\Delta t) \approx e^{\hat{A}_2 \frac{\Delta t}{2}} e^{\hat{A}_1 \frac{\Delta t}{2}} (e^{\hat{A}_1 \frac{\Delta t}{2}} e^{\hat{A}_2 \frac{\Delta t}{2}} u(t)) = e^{\hat{A}_2 \frac{\Delta t}{2}} e^{\hat{A}_1 \Delta t} e^{\hat{A}_2 \frac{\Delta t}{2}} u(t), \tag{2.5.7}$$

to increase the accuracy by an order. The symmetric splittings, (2.5.6) and (2.5.7), are called *Strang splitting* proposed by Strang (1968). The local truncation error of Strang splitting can be found by the Baker-Campbell-Hausdorff formula, too. After a time step Δt, the Strang splitting give rise to the local truncation error of

$$\Delta t^3 \Big(\frac{1}{12} [\hat{A}_2, [\hat{A}_2, \hat{A}_1]] - \frac{1}{24} [\hat{A}_1, [\hat{A}_1, \hat{A}_2]] \Big) u(t) + O(\Delta t^4). \tag{2.5.8}$$

The local truncation error (2.5.8) has no Δt^2 term, so the Strang splitting is accurate in the second order. If $\hat{A}_1$ and $\hat{A}_2$ commute, all splittings form are exact.

2.5.2 Extension for Time-Dependent Schrödinger Equation

The split operator method help to solve the following time-dependent Schrödinger equation (TDSE),

$$i \frac{\partial}{\partial t} \psi(\mathbf{r}, t) = \hat{H} \psi(\mathbf{r}, t). \tag{2.5.9}$$

The total Hamiltonian operator $\hat{H}$ may be decomposed into the time-independent operator $\hat{H}^0(\mathbf{r})$ and time-dependent operator $\hat{V}(\mathbf{r}, t)$.

$$i \frac{\partial}{\partial t} \psi(\mathbf{r}, t) = (\hat{H}^0 + \hat{V}) \psi(\mathbf{r}, t) \tag{2.5.10}$$

For the present research for the target atom, the $\hat{H}^0$ is the Hamiltonian of hydrogen atom with the variable change of radial part, $u(r) = rR(r)$.

$$\hat{H}^0(\mathbf{r}) = -\frac{1}{2} \frac{d^2}{dr^2} + \frac{\hat{L}^2}{2r^2} - \frac{1}{r} \tag{2.5.11}$$

where $\hat{L}^2$ is the angular momentum operator. For the the intense field $\mathbf{E}$ injected along the z axis, the $\hat{V}$ is the interaction between the intense field and atom.

$$\hat{V}(\mathbf{r}, t) = \mathbf{E}(t) \cdot \mathbf{r} = (E_0 f_s(t) \hat{\mathbf{e}}_z) \cdot (r \hat{\mathbf{e}}_r) = E_0 r \cos\theta f_s(t) \tag{2.5.12}$$

which E_0 is the amplitude of field, and $f_s(t)$ is the shape of field. The whole equation (2.5.10) describes the time evolution of states of hydrogen atom in the intense field.

Now extend the Strang splitting in spherical coordinates to the time propagation of the Schrödinger equation.

$$\psi(\mathbf{r}, t + \Delta t) \approx \exp(-i\hat{H}^0 \frac{\Delta t}{2}) \exp(-i\hat{V}\Delta t) \exp(-i\hat{H}^0 \frac{\Delta t}{2}) \psi(\mathbf{r}, t) \tag{2.5.13}$$

The time propagation of wave function ψ from t to $t + \Delta t$ is constructed from three steps to deal with the three operators.

I In energy space spanned by $\hat{H}^0$, the wave function $\psi(\mathbf{r}, t)$ is propagated half time step $\Delta t/2$

$$\psi_1(\mathbf{r}, t) = \exp(-i\hat{H}^0 \frac{\Delta t}{2}) \psi(\mathbf{r}, t) \tag{2.5.14}$$

II Afterwards the wave function $\psi(\mathbf{r}, t)$ is transformed back to the real space and propagated a time step Δt in the field **E**.

$$\psi_2(\mathbf{r}, t) = \exp(-i\hat{V}\Delta t) \psi_1(\mathbf{r}, t) \tag{2.5.15}$$

III At the end of one iteration, the wave function $\psi(\mathbf{r}, t)$ is transformed to the energy space spanned by $\hat{H}^0$ and propagated the other half time step $\Delta t/2$.

$$\psi(\mathbf{r}, t + \Delta t) = \exp(-i\hat{H}^0 \frac{\Delta t}{2}) \psi_2(\mathbf{r}, t) \tag{2.5.16}$$

With the scheme, **I** $\sim$ **III**, the simplest method to transform the wave function $\psi(\mathbf{r}, t)$ between real and energy space is the Fourier transform. After the transformation, the operator is a value in the space corresponding to the operator, so the work of operator on the wave function is the direct product of operator and the wave function. The work (Jiang and Chu, 1992) through the Fourier transform is a good example to apply split operator method in two-dimension.

2.5.3 Treatment of Hamiltonian Operator

Except the method to deal with the exponent operators in different space by Fourier transform, there is a other method to deal with both exponent operator, $\exp(-i\hat{H}^0\Delta t/2)$ and $\exp -(i\hat{V}\Delta t)$, in the real space. Tong and Chu (1997b) develop the method to deal

with the operator $\exp(-i\hat{H}^0\Delta t/2)$ in the real space by replacing the operator with its eigenvalues and eigenvectors. The method is derived explicitly in this subsection.

Due to the time-dependent field $E(\mathbf{r})$ along the z axis, the time evolution is independent of the azimuthal angle ϕ in spherical coordinates,

$$\psi(\mathbf{r}) = \psi(r, \theta), \tag{2.5.17}$$

and thus expand the wave function in spherical harmonics $Y_{lm}(\theta, \phi)$ with a given l, $l = 0$.

$$\psi(r, \theta) = \sum_l \frac{u_l(r)}{r} Y_{l,0}(\theta, \phi) \tag{2.5.18}$$

When the operator $\hat{H}^0$ works on the component $u_l(r)Y_{l,0}(\theta, \phi)$, the angular momentum operator $\hat{L}^2$ in $\hat{H}^0$ works on its eigenfunctions $Y_{l,0}(\theta, \phi)$ and gives its eigenvalues $-l(l+1)$. After the work of $\hat{L}^2$, the $\hat{H}^0$ denoted $\hat{H}^0_l$ only keeps the eigenvalue $-l(l+1)$.

$$\hat{H}^0_l(r) = \frac{1}{2}\frac{d^2}{dr^2} - \frac{l(l+1)}{2r^2} - \frac{1}{r} \tag{2.5.19}$$

The $\hat{H}^0_l(r)$ is the same as the operator in (2.3.34). All $\hat{H}^0_l(r)$ only depend on the radius r. Each component $u_l(r)/r$ gives a operator $\hat{H}^0_l(r)$ with the given l.

The eigenvalues $\epsilon_{k,l}$ and eigenfunctions $\chi_{n,l}(r)$ of $\hat{H}^0_l(r)$ working on the $u_l(r)$ are carried out by GPS in Subsection 2.3.3. $u_l(r)$ can be the linear combination of its normalized eigenvector $\chi_{n,l}(r)$.

$$u_l(r) = \sum_n c_n \chi_{nl}(r) \tag{2.5.20}$$

where the c_n are the coefficients and can found by the orthogonality of $\chi_{nl}(r)$.

$$c_n = \int \chi_{nl}(r) u_l(r) dr \tag{2.5.21}$$

Discretize r on the GLL grids, $r = r(x_j)$, by the mapping function (2.1.15), and c_n are in term of weighted sum by Gaussian quadrature.

$$c_n = \sum_j W_j \chi_{nl}(r(x_j)) u_l(r(x_j)) \frac{dr(x_j)}{dx} \tag{2.5.22}$$

Back to the expansion (2.5.18), let the operator $\exp(-i\hat{H}^0\Delta t/2)$ work on the wave function $\psi(r, \theta)$,

$$\exp(-i\hat{H}^0\frac{\Delta t}{2})\psi(r, \theta) = \exp(-i\hat{H}^0\frac{\Delta t}{2})\big[\sum_l u_l(r)Y_{l,0}(\theta, \phi)\big]. \tag{2.5.23}$$

After the $\hat{L}^2$ in $\hat{H}^0(\mathbf{r})$ is substituted by its eigenvalue, the $\hat{H}^0(\mathbf{r})$ of which the radial operator remains is denoted to $\hat{H}_l^0$ given by (2.5.19).

$$\exp(-i\hat{H}^0\frac{\Delta t}{2})\psi(r,\theta) = \sum_l \left[\exp(-i\hat{H}_l^0\frac{\Delta t}{2})u_l(r)\right]Y_{l,0}(\theta,\phi) \tag{2.5.24}$$

Focus on the square brackets. With the linear combination (2.5.20), the $\exp(-i\hat{H}_l^0\Delta t/2)$ further work on the eigenvectors $\chi_{n,l}$.

$$\exp(-i\hat{H}_l^0\frac{\Delta t}{2})u_l(r) = \sum_n c_n \exp(-i\hat{H}_l^0\frac{\Delta t}{2})\chi_{n,l}(r) \tag{2.5.25}$$

Replace the operator $\hat{H}_l^0$ on the exponent with its eigenvalues $\epsilon_{n,l}$.

$$\exp(-i\hat{H}_l^0\frac{\Delta t}{2})u_l(r) = \sum_n c_n \exp(-i\epsilon_{n,l}\frac{\Delta t}{2})\chi_{n,l}(r) \tag{2.5.26}$$

The coefficients c_n are given in (2.5.22).

$$\begin{aligned}&\exp(-i\hat{H}_l^0\frac{\Delta t}{2})u_l(r)\\ =&\sum_n[\sum_j W_j\chi_{n,l}(r(x_j))u_l(r(x_j))\frac{dr(x_j)}{dx}]\exp(-i\epsilon_{n,l}\frac{\Delta t}{2})\chi_{n,l}(r)\end{aligned} \tag{2.5.27}$$

Discretize r on GLL grids, $r = r(x_i)$, by the mapping function (2.1.15), and rearrange this equation.

$$\begin{aligned}&\exp(-i\hat{H}_l^0\frac{\Delta t}{2})u_l(r(x_i))\\ =&\sum_j[\sum_n \chi_{n,l}(r(x_i))\chi_{n,l}(r(x_j))\exp(-i\epsilon_{n,l}\frac{\Delta t}{2})W_j\frac{dr(x_j)}{dx}]u_l(r(x_j))\end{aligned} \tag{2.5.28}$$

Treat the square bracket as a matrix S. The elements of S are

$$S_{ij}(l) = \sum_k \chi_{k,l}(r(x_i))\chi_{k,l}(r(x_j))\exp(-i\epsilon_{k,l}\frac{\Delta t}{2})W_j\frac{dr(x_j)}{dx}. \tag{2.5.29}$$

The operator $\exp(-i\hat{H}_l^0\Delta t/2)$ now becomes a matrix-vector product of the matrix S and vector u_l.

$$\exp(-i\hat{H}_l^0\Delta t/2)u_l(r(x_i)) = \sum_j S_{ij}(l)u_l(r(x_j)) \tag{2.5.30}$$

The advantage of this method is all time propagation in the same space. It does need the Fourier transform. The difficulty is how to find the eigenvalues and eigenvectors of a operator.

2.5.4 Programming Scheme

The combination of Subsection 2.5.2 and Subsection 2.5.3 is actually used for the time propagation in the present research. The practical process of computation is concluded in the last subsection.

The wave function $\psi(\mathbf{r})$ is given in Subsection 2.5.2. The variation of wave function is independent of the azimuthal angle ϕ in spherical coordinates, so the Legendre polynomials $P_l(\cos\theta)$ can replace the spherical harmonics $Y_{l,0}(\theta,\phi)$ for expansion of $\psi(\mathbf{r})$. The radius r is discretized on the subset of GLL grids by the mapping function (2.1.15), and the inclination θ in cosine is discretized on GL grids (2.1.3). The number of the GLL girds may not equal to the number of GL girds.

In a time subinterval, $[t_k, t_{k+1}] = [t, t+\Delta t]$, start form the expansion of $\psi(\mathbf{r})$ in Legendre polynomials up to l_{max}.

$$\psi^0(r_i,\theta_j,t_k) = \sum_{l=0}^{l_{max}} u_l^0(r_i,t_k)P_l(\cos\theta_j) \tag{2.5.31}$$

The superscripts of u_l and ψ denote the order of steps. The r_i are the shorthand for $r(x_i)$. For the first step **I** in 2.5.2, compute the matrix-vector for each partial wave u_l to perform the work of the operator $\exp(-i\hat{H}^0\Delta/2)$.

$$u_l^1(r_i,t_k) = \sum_{j=1}^{N_{GLL}} S_{ij}(l)u_l^0(r_j) \tag{2.5.32}$$

Combine the radial part with angular part for the next step.

$$\psi^2(r_i,\cos\theta_j,t_k) = \sum_{l=0}^{l_{max}} u_l^1(r_i,t_k)P_l(\cos\theta_j) \tag{2.5.33}$$

For the second step **II** in 2.5.2, directly compute the product of the operator $\exp(-i\hat{V}\Delta t)$ and the wave function in real space.

$$\psi^3(r_i,\cos\theta_j,t_k) = \exp(-iV(r_i,\cos\theta_j,t_k+\frac{\Delta t}{2})\Delta t)\psi^2(r_i,\cos\theta_j,t_k) \tag{2.5.34}$$

where $V(r,\cos\theta,t)$ is defined by (2.5.12). Expand the $\psi^3(r,\cos\theta,t)$ in Legendre polynomials for the work of the other $\exp(-i\hat{H}^0\Delta/2)$.

$$u_l^4(r_i,t_k) = \frac{2l+1}{2}\sum_{j=1}^{N_{GL}} W_j\psi^3(r_i,\cos\theta_j,t_k)P_l(\cos\theta_j) \tag{2.5.35}$$

where the W_j are Gaussian weights on GL grids. For the third step **III**, compute the matrix-vector product for each partial wave u_l again.

$$u_l^0(r_i, t_{k+1}) = \sum_{j=1}^{N_{GLL}} S_{ij}(l) u_l^4(r_j) \tag{2.5.36}$$

The superscript returns to zero, and accomplish the time propagation in the time subinterval $[t_k, t_{k+1}]$.

After the step (2.5.36), the wave function $\psi(r, \theta, t_{k+1})$ is given. The remaining steps are the analysis from the given $\psi(r, \theta, t_{k+1})$.

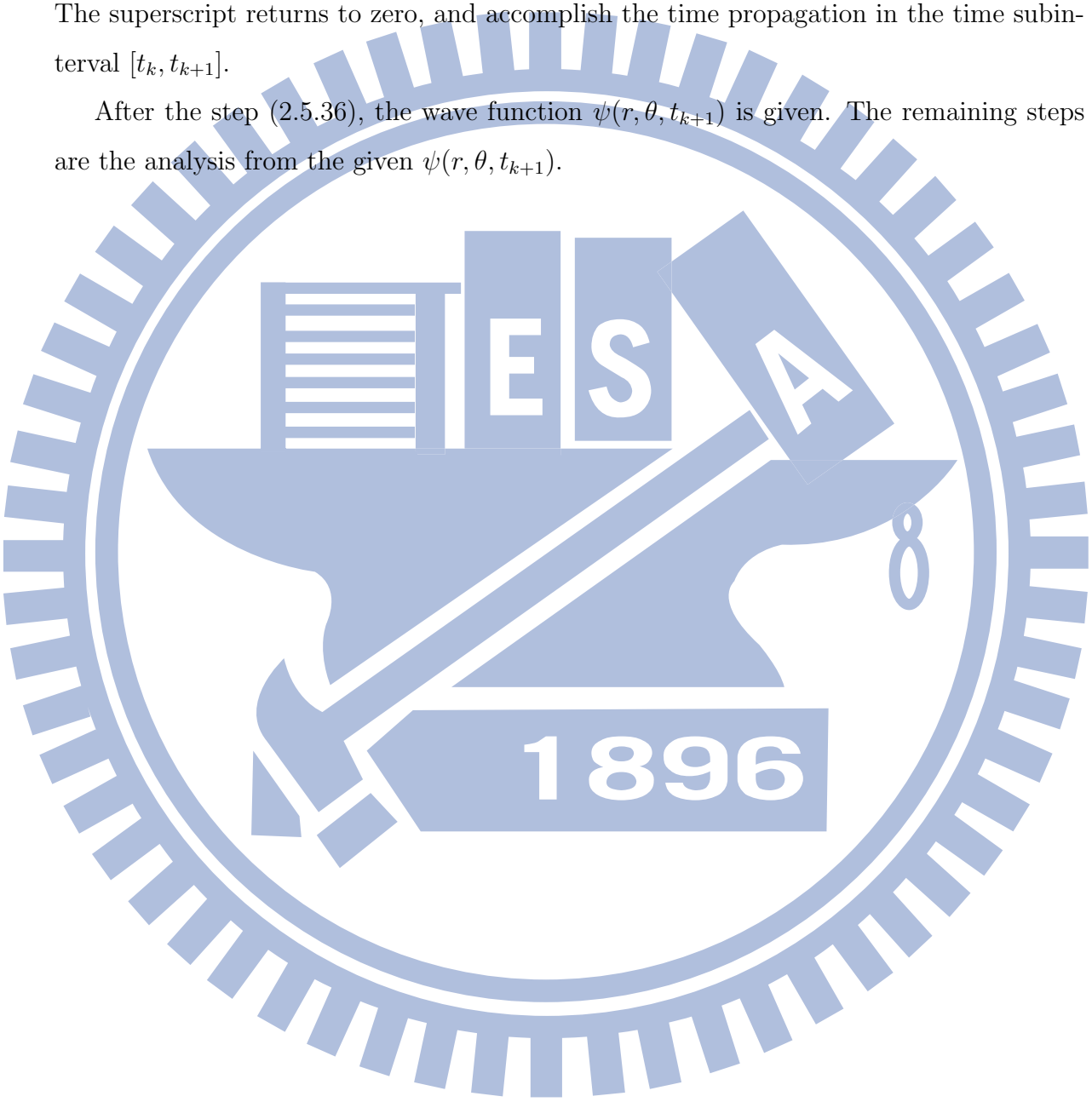

Chapter 3

Theory

3.1 Density Functional Theory (DFT)

Apply the Born-Oppenheimer approximation to a atomic system. Its Hamiltonian in atomic unit reads

$$H = \frac{1}{2}\sum_{i}^{N} p_i^2 + \frac{1}{2}\sum_{\substack{i,i'=1 \\ i\neq i'}}^{N} \frac{1}{|\mathbf{r}'_i - \mathbf{r}'_i|} - \frac{Z}{r} \tag{3.1.1}$$

where Z is the atomic number. For the such Hamiltonian, it is hard to find the analytical solution of the Schrödinger equation (SE). Even if use the numerical method to directly solve the SE, the computation become complex and take much time. The one of good approaches to deal with the Hamiltonian (3.1.1) is the density functional theory (DFT).

The DFT and related theories are developed for many years from the early 20th century. The DFT is generally employed in physics, chemical, and material. Many textbooks about DFT have been published. Parr and Yang (1989) give the DFT especially for atom and molecules. Kryachko and Ludena (1990) represent a strict framework and formalization of DFT and related theories in history. Martin (2004) has the modern applications of DFT to the electronic structure.

DFT is a tool in the present research and helps to deal with the many-electron system in term of the SE of individual electron. DFT is a huge theory, but this section do not cost much space to discuss DFT itself. This section only provides the fundamental theories, the concepts of exchange-correlation energy, and self-interaction correction.

3.1.1 Kohn-Sham Theorem

The fundamental of DFT is based on two articles, Hohenberg and Kohn (1964) and Kohn and Sham (1965). The fundamental theorems have two.

The first is that the density ρ is the basic variable. For a system in an external potential V, the potential V is unique unless the potential V is a constant, and determined by the particle density ρ in ground state.

The second is that a functional $E[\rho]$ for the energy E in term of the particle density ρ can be defined. The functional $E[\rho]$ is valid for any external potential V. The exact energy in ground state of this system is the global minimum value of the functional $E[\rho]$ with the particle density ρ which minimizes the functional $E[\rho]$ and is the exact particle density ρ_0.

In the present research, the particle refers the electron because the electrons denominate atomic system. The total density $\rho(\mathbf{r})$ and its components can be calculated via

$$\begin{aligned}\rho(\mathbf{r}) &= \sum_{\sigma}\sum_{i}^{N_\sigma} |\psi_{i\sigma}(\mathbf{r})|^2 = \sum_{\sigma}\sum_{i}^{N_\sigma} \rho_{i\sigma}(\mathbf{r}) \\ &= \rho_\uparrow(\mathbf{r}) + \rho_\downarrow(\mathbf{r}) = \sum_{i}^{N_\uparrow} |\psi_{i\uparrow}(\mathbf{r})|^2 + \sum_{i}^{N_\downarrow} |\psi_{i\downarrow}(\mathbf{r})|^2\end{aligned} \tag{3.1.2}$$

where σ is denoted the spin, and N_σ is the number of electrons with the same spin.

Based on the fundamental theorems, the total energy E in ground state of the interacting electrons is defined by a functional of the densities.

$$E[\rho_\uparrow, \rho_\downarrow] = T_s[\rho_\uparrow, \rho_\downarrow] + E_{ext}[\rho] + E_H[\rho] + E_{xc}[\rho_\uparrow, \rho_\downarrow] \tag{3.1.3}$$

Take the functional derivative of total energy E respect to the density $\rho(\mathbf{r})$ to find the minimization. The Kohn-Sham equation is obtained from the the variational equation of the functional derivative.

$$H_\sigma^{KS}\psi_{i\sigma}(\mathbf{r}) = \left[-\frac{1}{2}\nabla^2 + V_\sigma^{KS}\right]\psi_{i\sigma}(\mathbf{r}) = \epsilon_{i\sigma}\psi_{i\sigma}(\mathbf{r}) \tag{3.1.4}$$

where H_σ^{KS} is the Kohn-Sham effective Hamiltonian, and V_σ^{KS} is Kohn-Sham effective potential,

$$V_\sigma^{KS} = V_{ext}(\mathbf{r}) + V_H(\mathbf{r}) + V_{xc}(\mathbf{r}). \tag{3.1.5}$$

The Kohn-Sham equation (3.1.4) is a one-electron independent equation with the V_σ^{KS} constructed by the self-consistent solutions and gives the consistent solutions $\psi_{i\sigma}(\mathbf{r})$ also called (Kohn-Sham) orbitals.

With the the self-consistent solutions of (3.1.4), the components of E and V_σ^{KS} can be calculated. The first component of E is non-interacting kinetic energy T_s,

$$T_s[\rho_\uparrow, \rho_\downarrow] = \sum_\sigma \sum_i^{N_\sigma} \langle \psi_{i\sigma}(\mathbf{r}) \mid -\frac{1}{2}\nabla^2 \mid \psi_{i\sigma}(\mathbf{r}) \rangle. \tag{3.1.6}$$

The second component of E is the interaction energy E_{ext} of the electrons within the external potential $V_{ext}(\mathbf{r})$ assumed to be independent of spin.

$$E_{ext} = \int \rho(\mathbf{r}) V_{ext}(\mathbf{r}) d^3\mathbf{r}, \tag{3.1.7}$$

Without the injection of the additional field into the atomic system, the external potential for electrons is the Coulomb potential,

$$V_{ext}(\mathbf{r}) = -\frac{Z}{r} \tag{3.1.8}$$

due to the nucleus. The third component of E is the Hartree energy E_H. The Hartree energy E_H is the self-interaction energy due to the electron-electron repulsion.

$$E_H[\rho] = \frac{1}{2} \iint \frac{\rho(\mathbf{r})\rho(\mathbf{r}')}{|\mathbf{r} - \mathbf{r}'|} d^3\mathbf{r} d^3\mathbf{r}' \tag{3.1.9}$$

Its functional derivative is the Hartree potential V_H stated in Section 2.4.

$$V_H(\mathbf{r}) = \frac{\delta E_H[\rho]}{\delta \rho_\sigma(\mathbf{r})} = \int \frac{\rho(\mathbf{r}')}{|\mathbf{r} - \mathbf{r}'|} d^3\mathbf{r}', \tag{3.1.10}$$

The last component of E is the exchange-correlation energy E_{xc}. The functional derivative of E_{xc} is the exchange-correlation potential V_{xc},

$$V_{xc,\sigma}(\mathbf{r}) = \frac{\delta E_{xc}[\rho_\uparrow, \rho_\downarrow]}{\delta \rho_\sigma(\mathbf{r})}. \tag{3.1.11}$$

Both E_{xc} and V_{xc} are quantum terms and discussed in the next subsection.

3.1.2 Exchange and Correlation Functionals

The exchange-correlation energy functionals are key for the accurate calculation. There are two classes of approximation introduced in this subsection.

The exchange-correlation energy E_{xc} is a sum of two distinct terms, exchange energy E_x and correlation energy E_c.

$$E_{xc}[\rho_\uparrow, \rho_\downarrow] = E_x[\rho_\uparrow, \rho_\downarrow] + E_c[\rho_\uparrow, \rho_\downarrow] \tag{3.1.12}$$

Both exchange and correlation terms are the quantum effects, so the Kohn-Sham calculation is a quantum treatment.

The exchange energy E_x comes from a exchange interaction between identical particles. There are two kinds of identical particles for the symmetry and antisymmetry. Our target particles, electrons, are fermions. The famous theory for the exchange interaction of fermions is the Pauli exclusion principle. In theory, the exchange interaction always lowers the energy. The exact exchange energy can be expressed in term of the orbitals $\psi_{i\sigma}(\mathbf{r})$.

$$E_x = -\frac{1}{2}\sum_{\sigma}\sum_{i,j}\int\int \frac{\psi^*_{i\sigma}(\mathbf{r})\psi_{i\sigma}(\mathbf{r}')\psi^*_{j\sigma}(\mathbf{r}')\psi_{j\sigma}(\mathbf{r})}{|\mathbf{r}-\mathbf{r}'|}d^3\mathbf{r}'d^3\mathbf{r} \tag{3.1.13}$$

Generally, the amount of exchange energy is less than the Hartree energy E_H or kinetic energy T_s.

The correlation energy E_c might be defined by the difference between the exact solution and a reference state, so the correlation energy has different definitions. The difference between the exact solution of Schrödinger Equation and the solution of Hartree-Fock equation may be a well-defined chose for the correlation energy E_c. The amount of correlation energy is less than the exchange energy.

The exchange-correlation energy functional must be approximated. The oldest approximation is local-density approximation (LDA) proposed by Kohn and Sham (1965). Kohn and Sham (1965) consider that the solid system can be frequently treated as the limit of homogeneous electron gas. In general, the LDA treats any inhomogeneous system locally as a homogeneous electron gas. It simply expresses the exchange-correlation energy E_{xc} of the inhomogeneous system as an integration over the exchange-correlation energy density,

$$E^{LDA}_{xc}[\rho] = \int \rho(\mathbf{r})\varepsilon^{homo}_{xc}(\rho(\mathbf{r}))d^3\mathbf{r} \tag{3.1.14}$$

where the ε^{homo}_{xc} is the energy density, and, at any point, the $\varepsilon^{homo}_{xc}(\rho(\mathbf{r}))$ is assumed to be the same as a homogeneous electron gas. The LDA is a universal functional of ρ, and it is independent of any physical parameter. Thus the LDA is easily applied to the arbitrarily inhomogeneous system.

LDA based on the assumption that the number of spin-up electrons is the same as the number of spin-down electrons. The assumption does not satisfy the actual applications generally. For the actual applications, the local spin-density approximation (LSDA) is implemented in more general. The spin-dependent version of LDA proposed by von Barth

and Hedin (1972) is

$$E_{xc}^{LSDA}[\rho_\uparrow, \rho_\downarrow] = \int \rho(\mathbf{r})\varepsilon_{xc}^{homo}(\rho_\uparrow(\mathbf{r}), \rho_\downarrow(\mathbf{r}))d^3\mathbf{r} \tag{3.1.15}$$

where the $\varepsilon_{xc}^{homo}(\rho_\uparrow(\mathbf{r}), \rho_\downarrow(\mathbf{r}))$ is the exchange-correlation energy per particle in homogeneous electron gas with the *spin-up* and *spin-down* densities, $\rho_\uparrow(\mathbf{r})$ and $\rho_\downarrow(\mathbf{r})$. With the work (Oliver and Perdew, 1979), the exchange energy E_x^{LSDA} in LSDA is

$$E_x^{LSDA}[\rho_\uparrow, \rho_\downarrow] = \frac{3}{4}(\frac{6}{\pi})^{\frac{1}{3}} \int (\rho_\uparrow^{\frac{4}{3}}(\mathbf{r}) + \rho_\downarrow^{\frac{4}{3}}(\mathbf{r}))d^3\mathbf{r} \tag{3.1.16}$$

in term of $\rho_\uparrow$ and $\rho_\downarrow$. It can also be in term of the spin polar parameter,

$$\zeta(\mathbf{r}) = \frac{\rho_\uparrow(\mathbf{r}) - \rho_\downarrow(\mathbf{r})}{\rho(\mathbf{r})} = \frac{\rho_\uparrow(\mathbf{r}) - \rho_\downarrow(\mathbf{r})}{\rho_\uparrow(\mathbf{r}) + \rho_\downarrow(\mathbf{r})}. \tag{3.1.17}$$

For the Kohn-Sham calculation in the present research, the exchange potential V_x referred to LSDA is the $X\alpha$ potential (Slater et al., 1969),

$$V_x^{X\alpha}(\mathbf{r}) = -\frac{3}{2}\alpha[\frac{6}{\pi}\rho_\sigma(\mathbf{r})]^{\frac{1}{3}} \tag{3.1.18}$$

with an adjustable coefficient α. The correlation energy E_c and potential V_c are not completely known in analytic form, but they can be found by quantum Monte Carlo calculation and parametrized to use. Perdew-Zunger (ZP81) are the parametrized correlation energy and potential referred to LSDA in the present research. ZP81 is based on the numerical results (Ceperley, 1978; Ceperley and Alder, 1980) by quantum Monte Carlo calculation and parametrized by Perdew and Zunger (1981).

To improve the LSDA, not only the local density but also its gradients are added into the construction of exchange-correlation functionals. In fact, after actual work, the higher-order gradients do not raise the improvement of LSDA and even make worse. If only keep the first-order gradient in approximation to save the lost property of LSDA, the approximation is called generalized-gradient approximation (GGA). GGA is a class of exchange-correlation functionals, and its general form is

$$E_{xc}^{GGA}[\rho_\uparrow, \rho_\downarrow] = \int \rho(\mathbf{r})\varepsilon_{xc}(\rho_\uparrow(\mathbf{r}), \rho_\downarrow(\mathbf{r}), \nabla\rho_\uparrow(\mathbf{r}), \nabla\rho_\downarrow(\mathbf{r}))d^3\mathbf{r}. \tag{3.1.19}$$

Over many years, various GGAs are developed. For the Kohn-Sham calculations in the present research, The functional referred to GGA is the non-empirical GGA, PBE (Perdew et al., 1996; Perdew et al., 1997). PBE is one of the most popular GGA functionals. It satisfies the properties as many as possible and retains the correct feature of LSD when add others.

3.1.3 Optimized Effective Potential (OEP)

Except the approximation of functional, we also can get the better exchange-correlation potential through the optimized effective potential (OEP) method. The OEP leads to an integral equation which it is hard to solve. The integral equation can be approximated and become a system of linear equation. The simple introduction to OEP and the approximation for the integral equation are introduced in this subsection and the next subsection.

Because the effectively Kohn-Shan (KS) potential V_σ^{KS} is a functional of the spin-densities $\rho_\sigma(\mathbf{r})$, the KS orbitals $\psi_{i\sigma}(\mathbf{r})$ can also be written as a spin-densities functional $\psi_{i\sigma}[\rho_\sigma]$ if the KS orbitals $\psi_{i\sigma}(\mathbf{r})$ come from the Kohn-Sham equation with the V_σ^{KS}. By the relation (3.1.2), each explicit functional of density can be written as an explicit functional of orbital, but the each explicit functional of orbital may not be written as an explicit functional of density. The best example is the exchange energy (3.1.13).

By the same way, let the orbitals be the spin-densities functional, and the total energy can be written as

$$E[\rho_\sigma] = E[\{\psi_{i\sigma}[\rho_\sigma]\}] = E[\{\psi_{i\sigma}\}] \tag{3.1.20}$$

where the $\{\psi_{i\sigma}\}$ is a set of orbitals from the KS equation.

The fundamental theories point out the unique relation between the density ρ and the KS potential V_σ^{KS}. It can substitute the minimization of the total energy E with respect to $\rho(\mathbf{r})$ by the minimization of the total energy E with respect to V_σ^{KS}.

$$\frac{\delta E[\{\psi_{i\sigma}\}]}{\delta V_\sigma^{KS}} = 0 \tag{3.1.21}$$

Directly calculate the functional derivative by the chain rule.

$$\sum_{\sigma'}\sum_{i'}^{N_{\sigma'}}\int \frac{\delta E[\{\psi_{i\sigma}\}]}{\delta \psi_{i'\sigma'}(\mathbf{r}')}\frac{\delta \psi_{i'\sigma'}(\mathbf{r}')}{\delta V_\sigma^{KS}(\mathbf{r})}d^3\mathbf{r}' + c.c. = 0 \tag{3.1.22}$$

The derivation by Krieger et al. (1992a) gives

$$\sum_i \int [V_{xc,\sigma}(\mathbf{r}') - v_{xc,i\sigma}(\mathbf{r}')]\psi_{i\sigma}(\mathbf{r})\psi_{i\sigma}^*(\mathbf{r}')G_{j\sigma}(\mathbf{r},\mathbf{r}')d^3\mathbf{r}' + c.c. = 0 \tag{3.1.23}$$

where $v_{xc,i\sigma}(\mathbf{r})$ is the orbital-dependent potential,

$$v_{xc,i\sigma}(\mathbf{r}) = \frac{1}{\psi_{i\sigma}^*(\mathbf{r})}\frac{\delta E_{xc}[\{\psi_{i\sigma}\}]}{\delta \psi_{i\sigma}(\mathbf{r})}, \tag{3.1.24}$$

and $G_{j\sigma}(\mathbf{r},\mathbf{r}')$ is the Green's function,

$$G_{j\sigma}(\mathbf{r},\mathbf{r}') = \sum_{\substack{k \\ k\neq j}}^{\infty} \frac{\psi_{k\sigma}(\mathbf{r}')\psi^*_{k\sigma}(\mathbf{r})}{\epsilon_{j\sigma} - \epsilon_{k\sigma}}. \tag{3.1.25}$$

The integral equation (3.1.23) is the OEP equation. It allows to calculate the exchange-correlation potential $V_{xc,i\sigma}(\mathbf{r})$ for the given KS orbitals through the solution of (3.1.23).

OEP brings the improvements of the exchange-correlation potential. The most important improvement is the correction to the self-interaction contribution due to E_H and the approximation of E_{xc} in (3.1.3). The correction make $V_{xc,i\sigma}(\mathbf{r})$ have the right asymptotic behavior for $r \to \infty$ like a static electric potential of a charge, which means

$$V_{xc,i\sigma}(\mathbf{r}) \to -\frac{1}{r} \quad \text{when} \quad r \to \infty \tag{3.1.26}$$

for the behavior of the exact exchange potential. The other improvements are shown in the next chapter.

3.1.4 Krieger-Li-Iafrate Approximation (KLI)

Krieger, Li, and Iafrate (1990, 1992a, 1992b, 1993) offer an approximation to the integral equation (3.1.23). The approximation is called **KLI approximation**.

The KLI approximation gives that

$$V^{KLI}_{OEP,\sigma}(\mathbf{r}) = V_{ext}(\mathbf{r}) + \int \frac{\rho(\mathbf{r}')}{|\mathbf{r}-\mathbf{r}'|} d^3\mathbf{r}' + \frac{\delta E_{xc}[\rho_\uparrow,\rho_\downarrow]}{\delta\rho_\sigma(\mathbf{r})} + V^{KLI}_\sigma(\mathbf{r}) \tag{3.1.27}$$

where

$$V^{KLI}_\sigma(\mathbf{r}) = \sum_i \frac{\rho_{i\sigma}(\mathbf{r})}{\rho_\sigma(\mathbf{r})} v_{xc,i\sigma}(\mathbf{r}) + \sum_{\substack{i \\ i\neq N_\sigma}} \frac{\rho_{i\sigma}(\mathbf{r})}{\rho_\sigma(\mathbf{r})} (\overline{V}^{KLI}_{i\sigma} - \overline{v}_{xc,i\sigma}). \tag{3.1.28}$$

In (3.1.28), the $v_{xc,i\sigma}(\mathbf{r})$ is defined by (3.1.24). When we take the E_{xc} as an exact exchange energy E_x given in (3.1.13), the $v_{xc,i\sigma}(\mathbf{r})$ is the effectively spin-unrestricted potential of single particle,

$$v_{xc,i\sigma}(\mathbf{r}) = -\int \frac{\rho_{i\sigma}(\mathbf{r}')}{|\mathbf{r}-\mathbf{r}'|} d^3\mathbf{r}' - \frac{\delta E_{xc}[\rho_{i\sigma}]}{\delta\rho_{i\sigma}(\mathbf{r})}. \tag{3.1.29}$$

The $\overline{V}^{KLI}_{xc,i\sigma}$ and $\overline{v}_{xc,i\sigma}$ are the expectation of $V^{KLI}_{xc,i\sigma}$ and $v_{xc,i\sigma}(\mathbf{r})$.

$$\overline{V}^{KLI}_{i\sigma} = \langle \psi_{i\sigma} | V^{KLI}_\sigma | \psi_{i\sigma} \rangle \tag{3.1.30}$$

$$\overline{v}_{xc,i\sigma} = \langle \psi_{i\sigma} | v_{xc,i\sigma} | \psi_{i\sigma} \rangle \tag{3.1.31}$$

KLI approximation suggests that $(\overline{V}_{i\sigma}^{KLI} - \overline{v}_{xc,i\sigma})$ can be calculated through a solution of following linear system,

$$\sum_{j=1}^{N_\sigma - 1} (\delta_{ij\sigma} - M_{ij\sigma})(\overline{V}_{j\sigma}^{KLI} - \overline{v}_{xc,j\sigma}) = \overline{V}_{i\sigma}^{s} - \overline{v_{xc,i\sigma}} \qquad (3.1.32)$$

$$i = 1, 2, \ldots, N_\sigma - 1$$

where

$$M_{ij,\sigma} = \int \frac{\rho_{i\sigma}(\mathbf{r})\rho_{j\sigma}(\mathbf{r})}{\rho_\sigma(\mathbf{r})} d^3\mathbf{r} \qquad (3.1.33)$$

and,

$$\overline{V}_{i\sigma}^{s} = \langle \psi_{i\sigma} | \sum_{j}^{N_\sigma} \frac{\rho_{j\sigma}(\mathbf{r}) v_{xc,j\sigma}(\mathbf{r})}{\rho_\sigma(\mathbf{r})} | \psi_{i\sigma} \rangle. \qquad (3.1.34)$$

Tong and Chu (1997a) suggest the other way to treat $\overline{V}_{i\sigma}^{KLI}$. Directly use V_σ^{KLI} in previous iteration to calculate $\overline{V}_{i\sigma}^{KLI}$ without solving the linear system (3.1.32), and it is solved self-consistently with the equation (3.1.27). Both ways lead to converged result.

In KLI approximation, The exchange energy E_x^{KLI} is defined as

$$E_x^{KLI} = E_x[\rho_\uparrow, \rho_\downarrow] - \sum_\sigma \sum_i^{N_\sigma} \{E_H[\rho_{i\sigma}] + E_x[\rho_{i\sigma}]\}, \qquad (3.1.35)$$

the correlation energy E_c^{KLI} is defined as

$$E_c^{KLI} = E_c[\rho_\uparrow, \rho_\downarrow] - \sum_\sigma \sum_i^{N_\sigma} \{E_c[\rho_{i\sigma}]\}, \qquad (3.1.36)$$

and the total energy E^{OEP} by OEP method becomes

$$E^{OEP}[\{\psi_{i\sigma}\}] = E[\{\psi_{i\sigma}\}] - \sum_\sigma \sum_i^{N_\sigma} \{E_H[\rho_{i\sigma}] + E_{xc}[\rho_{i\sigma}]\}. \qquad (3.1.37)$$

Chapter 4

Results and Discussion

The results are divided into two sections by the time-dependent and time-independent calculation.

4.1 Kohn-Sham Calculation of Neutral Atom

The first section is the time-independent calculations. It is mainly to self-consistently solve the Kohn-Sham equation.

4.1.1 Kohn-Sham Calculation with Various Functionals

We first represent the basic Kohn-Sham (KS) calculation without optimized effective potential (OEP). From the KS calculations, we numerically calculated the total energies and exchange-correlation energies.

The specification for the present calculations is stated as follows. Discretized the r domain, $[0, r_{max}]$, on GLL grids by the mapping function (2.1.15). The number of the GLL grids was 103 for $Z = 1 - 2$ and 203 for $Z = 3 - 4$. The maximum radius r_{max} was $100\,a.u.$ for $Z = 1-2$ and $200\,a.u.$ for $Z = 3-4$. The length scale L was 20 for $Z = 1-4$. The L and r_{max} which keep within a proper range do not affect the result.

For the KS calculations, we used two classes of exchange-correlation functionals, LSDA and GGA. For the LSDA, the exchange energy and potential were (3.1.16) and $X\alpha$ potential (3.1.18) with $\alpha = 2/3$, and the correlation energy and potential were the parametrization ZP81 (Perdew and Zunger, 1981). For the GGA, we directly used the subroutine [1]. It

[1] It can be downloaded from their website http://dft.uci.edu/index.php

follows the instruction of Perdew et al. (1996). The KS equation was solved by GPS, and the iteration for the self-consistent solution had 20 times. One sequential computation only took few seconds by a modern computer.

Table 4.1.1 contains the total energies from KS calculations without the OEP and the exact values (Davidson et al., 1991). The LSDA underestimates the total energies, and its relative errors are in the $1-4\%$ range. The most relative error for hydrogen atom is about 4%. The LSDA may be useful in actual application to solid, but it may not enough accurate to predict an atomic system.

The GGA also underestimates the total energise, but the total energies by GGA are more closer to the exact values than the total energies by LSDA. All relative errors are less than 1%. GGA has good properties in the estimation of total energies.

Table 4.1.1: Total energies (in atomic units) of atoms (Z=1-4) from the Kohn-Sham calculations by the different exchange-correlation functionals, LSDA and GGA.

Z	Atom	LSDA	GGA	Exact[a]
1	H	−0.4789	−0.5000	−0.5000
2	He	−2.8343	−2.9029	−2.9037
3	Li	−7.3422	−7.4745	−7.4781
4	Be	−14.4462	−14.6664	−14.6674

[a] Davidson et al. (1991)

Table 4.1.2 contains the exchange energies from KS calculations with $X\alpha$ potential, PBE, and the results numerically calculated by Kurth et al. (1999). The exchange energies are underestimated by LSDA. The relative errors are in the range, $14-17\%$. Our results of LSDA are in good agreement with the other work (Kurth et al., 1999). The LSDA always has the typical error.

GGA significantly reduces the relative errors. All relative errors are less than 5%, and the smallest one is about 1%. As similar as the results of LSDA, Our results of GGA are in good agreement with the other work (Kurth et al., 1999), so our calculation is reliable.

Table 4.1.2: Exchange energies (in atomic units) of atoms (Z=1-4) from the Kohn-Sham calculations by the different exchange functionals, LSDA and GGA.

Z	Atom	LSDA	LSDA[a]	PBE	PBE[a]	Exact[b]
1	H	−0.2564	0.2680	−0.3018	−0.3059	−0.3125
2	He	−0.8617	0.8840	−1.0051	−1.0136	−1.0258
3	Li	−1.5179	1.5379	−1.7513	−1.7572	−1.7807
4	Be	−2.2905	2.3124	−2.6336	−2.6358	−2.6658

[a] Kurth et al. (1999)

[b] Exact result are numerically calculated from (3.1.13) by Kurth et al. (1999).

Table 4.1.3 contains the correlation energies from KS calculations with ZP81, PBE, and the results numerically calculated by Kurth et al. (1999). The magnitudes are almost identical in our work and the work of Kurth et al. (1999)

The relative errors for correlation energy are much more than the relative errors for exchange energy. LSDA overestimates the correlation energies by over 300% even if accurate parametrization, ZP81, is used. GGA reduces the relative errors to about 1.5% except the hydrogen atom. The ideal correlation functional does not give the correlation energy for hydrogen atom.

Table 4.1.3: Correlation energies (in atomic units) of atoms (Z=1-4) from the Kohn-Sham calculations by the different exchange-correlation functionals, LSDA and GGA.

Z	Atom	LSDA	LSDA[a]	PBE	PBE[a]	Exact [b]
1	H	−0.0218	−0.0222	−0.0057	−0.0060	−0.0000
2	He	−0.1109	−0.1125	−0.0411	−0.0420	−0.0420
3	Li	−0.1498	−0.1508	−0.0510	−0.0514	−0.0455
4	Be	−0.2234	−0.2240	−0.0854	−0.0856	−0.0950

[a] Kurth et al. (1999)

[b] Krieger et al. (1999)

4.1.2 Kohn-Sham Calculation with OEP Method and KLI Approximation

For the present calculations in this subsection, we applied the OEP method and the KLI approximation to find the correct potential and used it to make the calculations more accurate. The most conditions of numerical calculations were the same as the conditions of Subsection 4.1.1. The only difference was that we did not use the correlation functional. It let us to construct the single-particle potential through (3.1.29) in KLI procedure more easily.

Table 4.1.4 contains the exchange energies from exchange-only KS calculations. The letter 'a' is denoted the KLI procedure through the iteration of V_σ^{KLI}, and letter 'b' is denoted the KLI procedure through the traditional way to solve the system of linear equations. The results by LSDA without the correlation energy and OEP perfectly match the results of Chen et al. (1996). the LSDA underestimates the total energy by about $3-8\%$.

Table 4.1.4: Total energies (in atomic unit) for atoms (Z=1-4) from KS calculations with the exchange-only functional through the OEP method and KLI approximation.

Z	Atom	LSDA	LSDA[c]	KLI-LSDA[a]	KLI-LSDA[b]	KLI-LSDA[c]	Exact[d]
1	H	−0.4571	−0.4571	−0.5000	−0.5000	−0.5000	−0.5000
2	He	−2.7236	−2.7236	−2.8717	−2.8717	−2.8617	−2.9037
3	Li	−7.1934	−7.1934	−7.4437	−7.4466	−7.4342	−7.4781
4	Be	−14.2233	14.2233	−14.5977	−14.6033	−14.5795	−14.6674

[a] the KLI procedure through the iteration of V_σ^{KLI}.

[b] the KLI procedure through the traditional way to solve the linear system.

[c] Chen et al. (1996)

[d] Davidson et al. (1991)

With the performance of OEP method and KLI approximation, the relative errors are significantly reduced to $0-1\%$. Especially for hydrogen atom, the relative error is 0%. Not surprisingly the V_σ^{KLI} is equal to the sum of V_H and V_{xc} without correlation functional. They have opposite signs and cancel each other in (3.1.27). The KS equation becomes the Schrödinger equation of hydrogen atom with $l=0$. The total energies ($Z=2-4$) may be

the best results as shown in Table 4.1.4 because of the KS calculations with exchange-only.

Table 4.1.5 contains the highest occupied atomic orbital (HOAO) energies from the KS calculations with exchange-only functional. In orbital-dependent DFT, the HOAO energy directly from the eigenvalues of KS equation should be equal to the ionization energy. The ionization energy is noticeably smaller than the experimental value by about 50% because LSDA without the OEP has the incorrect long-range behavior. With the implement of the OEP methods and KLI approximation, the results are improved, and the relative errors reduced to $0-5\%$. Comparing with the work of Chen et al. (1996), our values ($Z=2,4$) are better in accuracy, but the other value ($Z=3$) is worse.

Table 4.1.5: Highest occupied orbital energies (in atomic unit) for atoms (Z=1-4) from KS calculations with the exchange-only functional through the OEP method and KLi approximation.

Z	Atom	LSDA	LSDA[c]	KLI-LSDA[a]	KLI-LSDA[b]	KLI-LSDA[c]	Exact[d]
1	H	−0.2469	−0.2690	−0.5000	−0.5000	−0.5000	−0.5000
2	He	−0.5170	−0.5703	−0.9280	−0.9280	−0.9481	−0.9036
3	Li	−0.1004	−0.1163	−0.2262	−0.2206	−0.1973	−0.1981
4	Be	−0.1700	−0.2058	−0.3448	−0.3390	−0.3285	−0.3426

[a] the KLI procedure through the iteration of V_σ^{KLI}.

[b] the KLI procedure through the traditional way to solve the linear system.

[c] reference Chen et al. (1996)

[d] Z=2-4 from reference Kramida et al. (2014)

We carried out the results shown in Table 4.1.4 and Table 4.1.5, and compared the values with other works. On the whole, the KLI procedure is good approximation to OEP for the improving of the LSDA energy functional.

To perform the KLI procedure, we used the method to iterate the V_σ^{KLI} and the traditional method to solve the linear system, and both methods led to the ideal results shown in Table 4.1.4 and Table 4.1.5. The difference between them is very small. We confirmed the suggestion of Tong and Chu (1997a). The method to iterate the V_σ^{KLI} is a simplified way to perform the KLI procedure.

4.2 Hydrogen Atom in Intense Laser Fields

This section shows the time-dependent calculation. It is mainly to solve the time-dependent Schrödinger equation (TDSE).

Recall Subsection 2.5.2. We assumed that the intense field $\mathbf{E}$ in (2.5.12) is subjected into the system along the z-axis.

$$\mathbf{E}(t) = E_0 f_s(t)\hat{\mathbf{e}}_z \tag{4.2.1}$$

where E_0 is the field amplitude, and $f_s(t)$ is a envelop function which models the intense evolution of $\mathbf{E}$. For the time-dependent calculations, we chose a ramped function to reasonable simulate the unstable output when we turn on the device producing the intense field in a experiment. The form of the ramped function is

$$f_s(t) = \begin{cases} \sin^2(\frac{\pi t}{2T_0})\sin(\omega_0 t) & t \le T_0 \\ \sin(\omega_0 t) & T_0 \le t \end{cases} \tag{4.2.2}$$

where T_0 is the period from unstable output to stable output.

The intense field often refers to the laser. The laser wavelength λ and intense I were $775nm$ and $3 \times 10^{13} W\, cm^{-2}$. We converted the λ and I to ω_0 and E_0 in atomic unit.

$$\omega_0 = \frac{2\pi \times 3 \times 10^8}{\lambda \times 4.1341 \times 10^{16}} = 5.88 \times 10^{-2} \tag{4.2.3}$$

$$E_0 = -\sqrt{\frac{I}{3.51 \times 10^{16}}} = -2.92 \times 10^{-2} \tag{4.2.4}$$

4.2.1 High-Order Harmonic Generation (HHG)

To investigate HHG, the most straightforward strategy is the direct solution of TDSE. The specification for the calculation of TDSE is stated as follow. We used the mapping function (2.1.15) to discretize the finite interval $[0, r_{max}]$ on the GLL grids. There were 201 GLL grids without the end points, and we did not use the end points, $x = -1$ and $x = 1$, in the present calculations. The maximum radius r_{max} was $200\, a.u.$, and the length scale L was 100. The L in the present calculation is much larger than the L in the time-independent calculation in Section 4.1 because the wave spreads in the intense field. The wave function is expanded in Legendre polynomials, and the maximum l is 19.

A mask function was applied to the present calculations to avoid the reflection of the spreading wave. The mask function $f_m(r)$ is the cosine form,

$$f_m(r) = \begin{cases} 1 & r \leq r_0 \\ \cos^{\frac{1}{4}}(\dfrac{\pi(r-r_0)}{2(r_{max}-r_0)}) & r_0 \leq r \end{cases}. \tag{4.2.5}$$

The $f_m(r)$ makes the wave function gradually decay to 0 from r_0 to r_{max}. We used $r_0 = 100\, a.u.$ for the present calculations.

For the time propagation, we turned on the laser field. First 10 optical cycles were for turning on the laser, $T_0 = 10$. The wave function was propagated for 30 optical cycles under the intense field of the constant peak. There were total 40 optical cycles. A optical cycle was divided into 2000 time steps. The procedure of time propagation is identical to the procedure in Subsection 2.5.4.

Figure 4.2.1 shows the remaining probability of a hydrogen atom in the intense field **E**. The remaining probability $P_r(t)$ is calculated by

$$P_r(t) = \langle \Psi(r,t) | \Psi(r,t) \rangle. \tag{4.2.6}$$

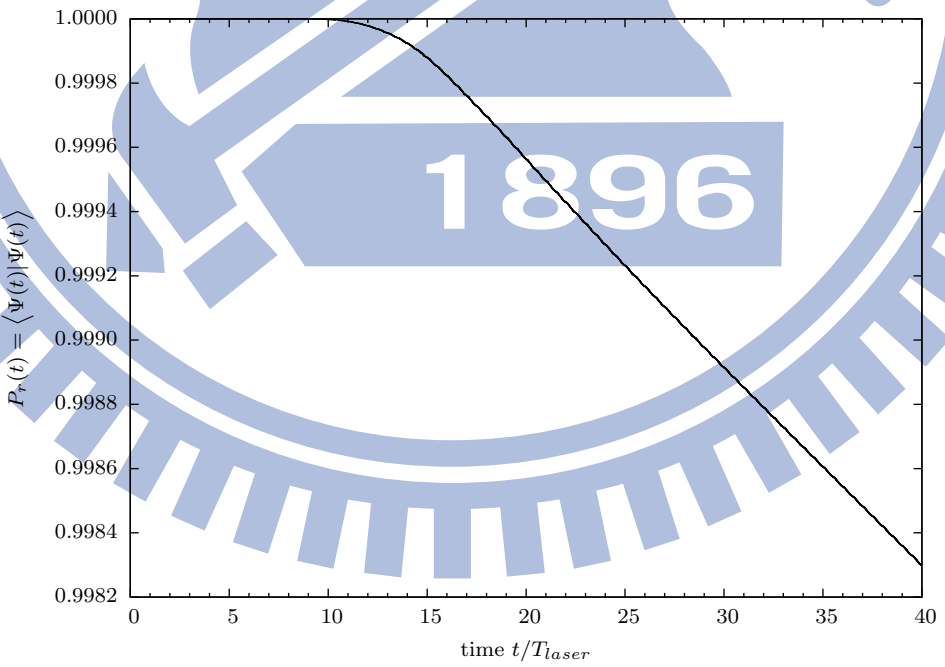

Figure 4.2.1: Remaining probability $P_r(t)$ of a hydrogen atom in the laser field of the wavelength $775\, nm$ and intensity $3 \times 10^{13}\, W/cm^2$ duration 40 optical cycles.

The P_r does not change for the first 10 optical cycles. After 10 optical cycles, the P_r decays slowly and linearly. When the time propagation end, $t = 40T$, P_r still keeps over 99 percent, and few electrons escape to free space. It means that we do not need to consider the electronic emission from the hydrogen atom.

Figure 4.2.2 displays the dipole moment induced in a hydrogen atom by the laser field $\mathbf{E}$. The dipole moments of length form and acceleration from can be calculated from the wave function $\psi(\mathbf{r}, t)$ at each time step as

$$d_L(t) = \langle \psi(\mathbf{r}, t) \mid z \mid \psi(\mathbf{r}, t) \rangle = \int \psi(\mathbf{r}, t) r \cos\theta \psi^*(\mathbf{r}, t) d^3\mathbf{r}, \tag{4.2.7}$$

$$d_A(t) = \langle \psi(\mathbf{r}, t) \mid -\frac{z}{r^3} + E_0 f_s(t) \mid \psi(\mathbf{r}, t) \rangle = \int \psi(\mathbf{r}, t)[-\frac{z}{r^3} + E_0 f_s(t) \psi^*(\mathbf{r}, t)] d^3\mathbf{r}. \tag{4.2.8}$$

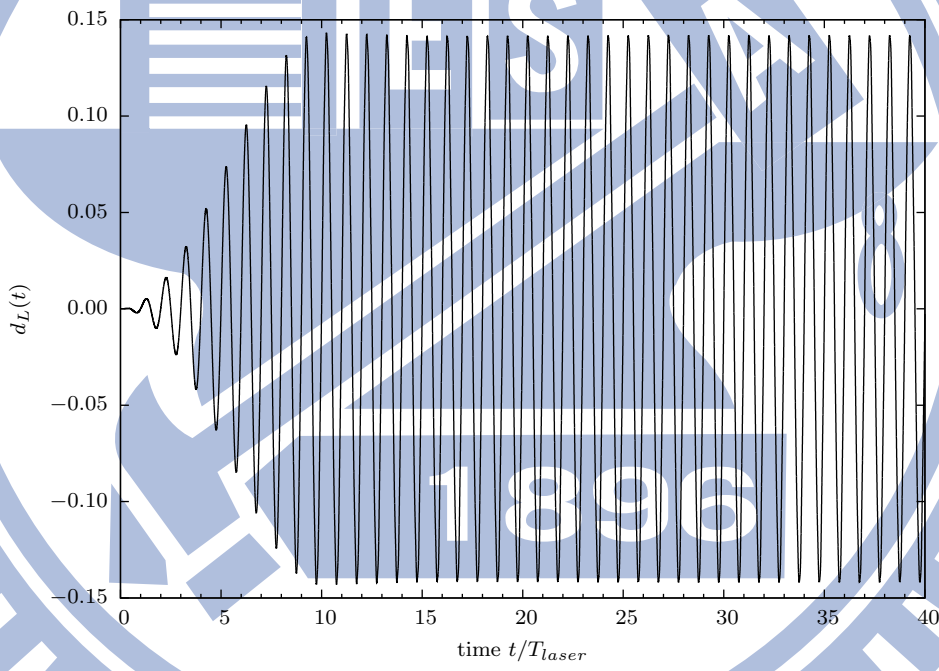

Figure 4.2.2: Length-form dipole $d_L(t)$ induced in a hydrogen atom by a laser field with the wavelength $775\,nm$ and intensity $3 \times 10^{13}\,W/cm^2$.

The dipole moment in length form oscillates with the variation of $f_s(t)$. The amplitude of oscillation is increasing during the first 10 optical cycles and keeps the constant amplitude during the last 30 optical cycles.

Figure 4.2.3 shows the power (harmonic) spectrum of HHG of a hydrogen atom by the laser field. The power spectra, $P_L(\omega)$ and $P_A(\omega)$, are square of Fourier transform of

the dipole momentums, $d_L(t)$ and $d_A(t)$.

$$P_L(\omega) = \left| \frac{1}{T_2 - T_1} \int_{T_1}^{T_2} d_L(t) e^{-i\omega t} dt \right|^2 \tag{4.2.9}$$

$$P_A(\omega) = \left| \frac{1}{(T_2 - T_1)\omega^2} \int_{T_1}^{T_2} d_A(t) e^{-i\omega t} dt \right|^2 \tag{4.2.10}$$

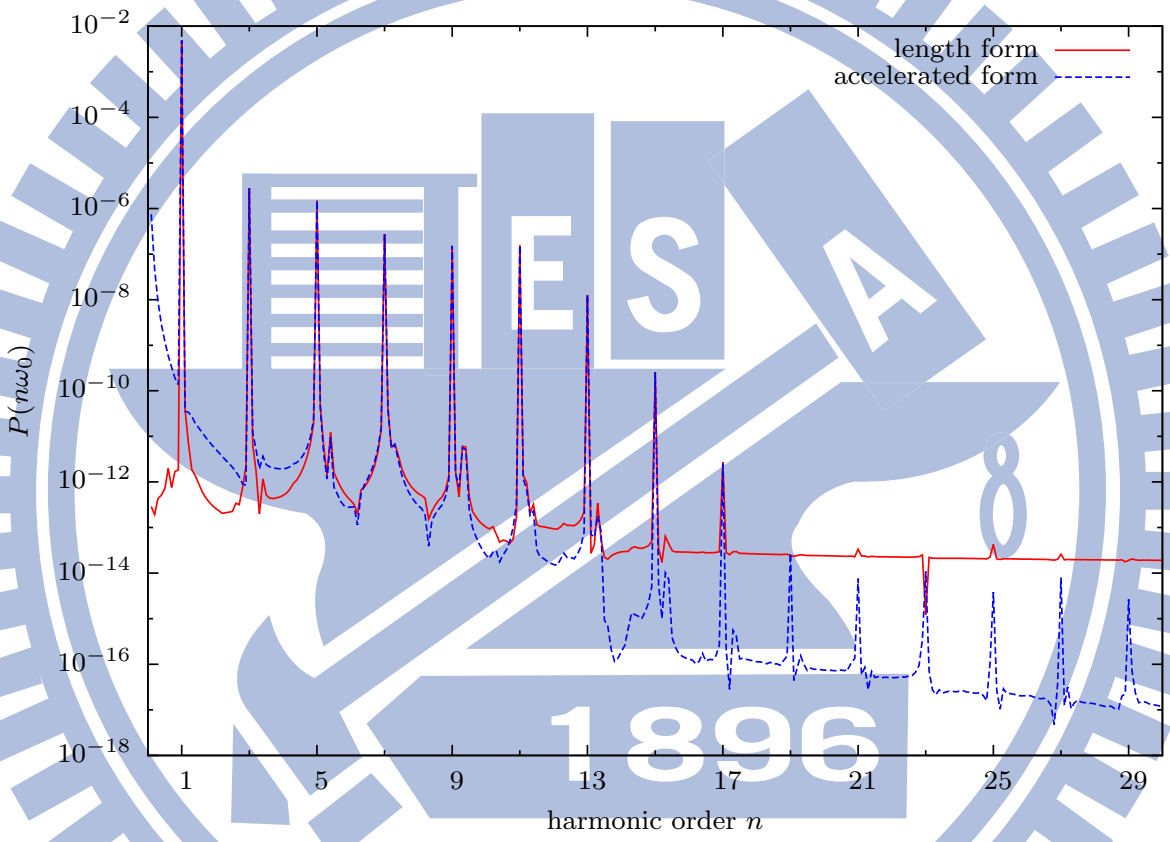

Figure 4.2.3: Harmonic spectrum obtained from the Fourier transform that takes 15 cycles from the 20th to the 35th cycle in figure 4.2.2.

We took 15 cycles from the 20th to the 35th cycle to perform the Fourier transform and calculate the power spectra.

First we make sure the physics process of ionization. For the time-dependent system, the ponderomotive energy U_p and ionization energy E_I are $U_p \approx 0.062$ and $E_I = 0.5$ for a hydrogen atom. By the Keldysh parameter,

$$\gamma = \sqrt{\frac{E_I}{2U_p}} = \sqrt{\frac{0.5}{2.062}} \approx 2.00 >> 1, \tag{4.2.11}$$

the ionization is a multiphoton process and may lead to HHG.

In physics, the spectra (see Figure 4.2.3) provide some features about HHG. The difference between peaks is *twice* as large as the photon $\hbar\omega_0$. Only *odd* harmonic peaks occur in the power spectra. Both are the features of HHG and unchanged even if we change the parameters of simulation over a adapted range. The cut-off law can determine the maximum order by U_p and E_I,

$$E_{cut} = 3.17U_p + E_I. \tag{4.2.12}$$

For the spectra in Figure 4.2.3,

$$n\omega_0 = 3.17 \times 0.062 + 0.5 = 0.696 \tag{4.2.13}$$

n is about 12. It matches the fact that the values of peaks decay quickly from $n = 13$.

Tong and Chu (1997b) list the the peak values in their article. It can be compared with us to make sure the accuracy. The peak values in Figure 4.2.3 and the results of Tong and Chu (1997b) are listed in Table 4.2.1. The peak values, P_L and P_A ,converge to the same values. The peak values ($n = 3, 5, 9, 11$) on the plateau are in good agreement with the work (Tong and Chu, 1997b).

Table 4.2.1: Peak values in the HHG spectrum in Figure 4.2.3

n	$P_L(n\omega_0)$	$P_A(n\omega_0)$	$P_L(n\omega_0)$[a]	$P_A(n\omega_0)$[a]
3	2.77[−06]	2.78[−06]	2.77[−06]	2.75[−06]
5	1.48[−06]	1.48[−06]	1.04[−06]	1.04[−06]
7	2.71[−07]	2.71[−07]	6.46[−08]	6.54[−08]
9	1.51[−07]	1.51[−07]	1.65[−07]	1.65[−07]
11	1.54[−07]	1.54[−07]	1.51[−07]	1.51[−07]
13	1.25[−08]	1.27[−08]	1.34[−08]	1.34[−08]
15	2.59[−10]	2.51[−10]	2.37[−10]	2.43[−10]
17	2.74[−12]	2.51[−12]	1.98[−12]	1.83[−12]

[a] Work of Tong and Chu (1997b)

The extra topic is the computational speed. For the present calculation, there were 80000 time steps in a time propagation. The time propagation only took about 100 seconds by Graphic Processing Unit (GPU) accelerator.

Bibliography

Abramowitz, M. and I. A. Stegun (1972). *Handbook of Mathematical Functions With Formulas, Graphs, and Mathematical Tables*. Applied Mathematics Series. Dover Publications.

Bayliss, A., A. Class, and B. J. Matkowsky (1995). Roundoff error in computing derivatives using the chebyshev differentiation matrix. *Journal of Computational Physics 116*(2), 380 – 383.

Canuto, C., M. Y. Hussaini, A. Quarteroni, and T. A. Zang (1988). *Spectral Methods in Fluid Dynamics*. Springer Series in Computational Physics. Springer Berlin Heidelberg.

Canuto, C., A. Quarteroni, M. Y. Hussaini, and T. A. Z. Jr. (2007). *Spectral methods : evolution to complex geometries and applications to fluid dynamics*. Scientific Computation. Springer Berlin Heidelberg.

Ceperley, D. (1978, Oct). Ground state of the fermion one-component plasma: A monte carlo study in two and three dimensions. *Phys. Rev. B 18*, 3126–3138.

Ceperley, D. M. and B. J. Alder (1980, Aug). Ground state of the electron gas by a stochastic method. *Phys. Rev. Lett. 45*, 566–569.

Chen, J., J. B. Krieger, Y. Li, and G. J. Iafrate (1996, Nov). Kohn-sham calculations with self-interaction-corrected local-spin-density exchange-correlation energy functional for atomic systems. *Phys. Rev. A 54*, 3939–3947.

Davidson, E. R., S. A. Hagstrom, S. J. Chakravorty, V. M. Umar, and C. F. Fischer (1991, Dec). Ground-state correlation energies for two- to ten-electron atomic ions. *Phys. Rev. A 44*, 7071–7083.

Hohenberg, P. and W. Kohn (1964, Nov). Inhomogeneous electron gas. *Phys. Rev. 136*, B864–B871.

Jiang, T.-F. and S.-I. Chu (1992, Dec). High-order harmonic generation in atomic hydrogen at 248 nm: Dipole-moment versus acceleration spectrum. *Phys. Rev. A 46*, 7322–7324.

Jiang, T. F., X.-M. Tong, and S.-I. Chu (2001, Jan). Self-interaction-free density-functional theoretical study of the electronic structure of spherical and vertical quantum dots. *Phys. Rev. B 63*, 045317.

Kohn, W. and L. J. Sham (1965, Nov). Self-consistent equations including exchange and correlation effects. *Phys. Rev. 140*, A1133–A1138.

Kramida, A., Yu. Ralchenko, J. Reader, and and NIST ASD Team (2014). NIST Atomic Spectra Database (ver. 5.2), [Online]. Available: `http://physics.nist.gov/asd` [2014, November 26]. National Institute of Standards and Technology, Gaithersburg, MD.

Krause, J. L., K. J. Schafer, and K. C. Kulander (1992, Jun). High-order harmonic generation from atoms and ions in the high intensity regime. *Phys. Rev. Lett. 68*, 3535–3538.

Krieger, J., Y. Li, and G. Iafrate (1990). Derivation and application of an accurate kohn-sham potential with integer discontinuity. *Physics Letters A 146*(5), 256 – 260.

Krieger, J. B., J. Chen, G. J. Iafrate, and A. Savin (1999). Construction of an accurate self-interaction-corrected correlation energy functional based on an electron gas with a gap. In A. Gonis, N. Kioussis, and M. Ciftan (Eds.), *Electron Correlations and Materials Properties*. Springer US.

Krieger, J. B., Y. Li, and G. J. Iafrate (1992a, Jan). Construction and application of an accurate local spin-polarized kohn-sham potential with integer discontinuity: Exchange-only theory. *Phys. Rev. A 45*, 101–126.

Krieger, J. B., Y. Li, and G. J. Iafrate (1992b, Nov). Systematic approximations to the optimized effective potential: Application to orbital-density-functional theory. *Phys. Rev. A 46*, 5453–5458.

Kryachko, E. S. and E. V. Ludena (1990). *Energy Density Functional Theory of Many-Electron Systems*. Understanding Chemical Reactivity. Springer.

Kurth, S., J. P. Perdew, and P. Blaha (1999). Molecular and solid-state tests of density functional approximations: Lsd, ggas, and meta-ggas. *International Journal of Quantum Chemistry 75*(4-5), 889–909.

Li, Y., J. B. Krieger, and G. J. Iafrate (1993, Jan). Self-consistent calculations of atomic properties using self-interaction-free exchange-only kohn-sham potentials. *Phys. Rev. A 47*, 165–181.

Martin, R. M. (2004). *Electronic Structure: Basic Theory and Practical Methods*. Cambridge University Press.

Midorikawa, K. (2011). High-order harmonic generation and attosecond science. *Japanese Journal of Applied Physics 50*(9R), 090001.

Oliver, G. L. and J. P. Perdew (1979, Aug). Spin-density gradient expansion for the kinetic energy. *Phys. Rev. A 20*, 397–403.

Parr, R. G. and W. Yang (1989). *Density-Functional Theory of Atoms and Molecules*. International Series of Monographs on Chemistry. Oxford University Press.

Perdew, J. P., K. Burke, and M. Ernzerhof (1996, Oct). Generalized gradient approximation made simple. *Phys. Rev. Lett. 77*, 3865–3868.

Perdew, J. P., K. Burke, and M. Ernzerhof (1997, Feb). Generalized gradient approximation made simple [phys. rev. lett. 77, 3865 (1996)]. *Phys. Rev. Lett. 78*, 1396–1396.

Perdew, J. P. and A. Zunger (1981, May). Self-interaction correction to density-functional approximations for many-electron systems. *Phys. Rev. B 23*, 5048–5079.

Peyret, R. (2002). *Spectral Methods for Incompressible Viscous Flow*. Applied Mathematical Sciences. Springer.

Slater, J. C., T. M. Wilson, and J. H. Wood (1969, Mar). Comparison of several exchange potentials for electrons in the cu^+ ion. *Phys. Rev. 179*, 28–38.

Strang, G. (1968). On the construction and comparison of difference schemes. *SIAM Journal on Numerical Analysis 5*(3), 506–517.

Telnov, D. A. and S.-I. Chu (1999, Apr). Multiphoton detachment of H^- near the one-photon threshold: Exterior complex-scaling—generalized pseudospectral method for complex quasienergy resonances. *Phys. Rev. A 59*, 2864–2874.

Tong, X.-M. and S.-I. Chu (1997a, May). Density-functional theory with optimized effective potential and self-interaction correction for ground states and autoionizing resonances. *Phys. Rev. A 55*, 3406–3416.

Tong, X.-M. and S.-I. Chu (1997b). Theoretical study of multiple high-order harmonic generation by intense ultrashort pulsed laser fields: A new generalized pseudospectral time-dependent method. *Chemical Physics 217*(23), 119 – 130. Dynamics of Driven Quantum Systems.

Trotter, H. F. (1959). On the product of semi-groups of operators. *Proc. Amer. Math. Soc. 10*, 545–551.

von Barth, U. and L. Hedin (1972). A local exchange-correlation potential for the spin polarized case. i. *Journal of Physics C: Solid State Physics 5*(13), 1629.

Wang, J., S.-I. Chu, and C. Laughlin (1994, Oct). Multiphoton detachment of H^-. ii. intensity-dependent photodetachment rates and threshold behavior—complex-scaling generalized pseudospectral method. *Phys. Rev. A 50*, 3208–3215.

Wang, T.-J. and Z.-W. Yan (2012, Feb). A note to legendre-gauss-lobatto nodes. *Journal of Henan University of Science and Technology: Natural Science 33*(1).

Appendix A

Legendre Polynomials

Let

$$x = \cos\theta$$

Properties

$$P_N(\pm 1) = (\pm 1)^N \tag{A.0.1}$$

$$P'_N(\pm 1) = (\pm 1)^{N+1}\frac{N(N+1)}{2} \tag{A.0.2}$$

Recurrence Relation Following formula in term of $P_{l-1}(x)$ and $P_{l-2}(x)$ can be used to find the Legendre polynomial with any l through iteration.

$$P_l(x) = \frac{1}{l}[(2l-1)xP_{l-1}(x) - (l-1)P_{l-2}(x)] \tag{A.0.3}$$

Following formula can be used to find the 1st derivative of Legendre polynomial with any l by given $P_l(x)$ and $P_{l-1}(x)$.

$$P'_l(x) = \frac{1}{1-x^2}[-lxP_l(x) + lP_{l-1}(x)] \tag{A.0.4}$$

Following formula can be used to find the 2nd derivative of Legendre polynomial with any l by given $P'_l(x)$ and $P_l(x)$.

$$P''_l(x) = \frac{1}{1-x^2}[2xP'_l(x) - N(N+1)P_l(x)] \tag{A.0.5}$$

Following relation is used in the proof.

$$\frac{d}{dx}[(1-x^2)P'_l(x)] = [(1-x^2)P'_l(x)]' = -N(N+1)P_l(x) \tag{A.0.6}$$

Orthogonality

$$\int_{-1}^{1} P_l(x)P_{l'}(x)dx = \frac{2}{2l+1}\delta_{ll'} \tag{A.0.7}$$

Special Case Expand the differential term on left side of (A.0.6).

$$(1-2x)P_l'(x) + (1-x^2)P_l''(x) = -N(N+1)P_l(x) \tag{A.0.8}$$

On Gauss-Legendre-Lobatto grids, $x = x_i \neq x_0 \neq x_N$, the first term is zero because of $P_l'(x_i) = 0$.

$$(1-x_i^2)P_l''(x_i) = -N(N+1)P_l(x_i) \tag{A.0.9}$$

Rearrange the equation.

$$P_l''(x_i) = \frac{N(N+1)P_l(x_i)}{(x^2-1)} \tag{A.0.10}$$

Appendix B

Numerical Calculations of Gradient and Laplacian

In Kohn-Sham calculations, we need to numerically calculate the gradient of density $\rho(\mathbf{r})$ or Laplacian of orbital $\psi(\mathbf{r})$ for the parameters of generalized gradient approximation (GGA)

In spherical coordinates, the gradient and Laplacian generally read

$$\nabla = \frac{\partial}{\partial r}\hat{\mathbf{e}}_r + \frac{1}{r}\frac{\partial}{\partial \theta}\hat{\mathbf{e}}_\theta + \frac{1}{r\sin\theta}\frac{\partial}{\partial \phi}\hat{\mathbf{e}}_\phi, \tag{B.0.1}$$

and

$$\nabla^2 = \frac{1}{r^2}\frac{\partial}{\partial r}(r^2\frac{\partial}{\partial r}) + \frac{1}{r^2\sin\theta}\frac{\partial}{\partial \theta}(\sin\theta\frac{\partial}{\partial \theta}) + \frac{\partial^2}{\partial \phi^2}. \tag{B.0.2}$$

For the KS calculations in the present research, the orbitals and densities only have two variables, r and θ. The numerical method to find the derivative respect to radius r is provided in Subsection 2.2.4. This appendix provides the numerical differential with respect to polar angle θ.

First, we expand the density $\rho(\mathbf{r})$ in spherical harmonic with $m = 0$.

$$\rho(\mathbf{r}) = \rho(r,\theta) = \sum_l \rho_l(r) Y_{l,0}(\theta,\phi) \tag{B.0.3}$$

where the coefficient $\rho_l(r)$ is

$$\rho_l(r) = \int Y_{l,0}(\theta,\phi)\rho(r,\theta)\sin\theta d\Omega. \tag{B.0.4}$$

The spherical harmonics with $m = 0$ can be in term of the Legendre polynomials $P_l(x)$

$$Y_{l0} = \sqrt{\frac{2l+1}{4\pi}} P_l(x) \tag{B.0.5}$$

where $x = \cos\theta$. The expansion becomes

$$\rho(r,\theta) = \sum_l \frac{2l+1}{4\pi}\rho_l(r)P_l(x). \tag{B.0.6}$$

In the expansion, the radial and angular parts are separated. The differential operators with respect to θ only work on the angular part. Apply the chain rule

$$\frac{dP_l(x)}{d\theta} = \frac{dP_l(x)}{dx}\frac{dx}{d\theta} = -\sin\theta\frac{dP_l(x)}{dx} \tag{B.0.7}$$

The 2nd-order differential operator works on $P_l(x)$.

$$\begin{aligned}\frac{d^2P_l(x)}{d\theta^2} &= \frac{d}{d\theta}(-\sin\theta\frac{dP_l(x)}{dx}) \\ &= -\cos\theta\frac{dP_l(x)}{dx} - \sin\theta\frac{d}{d\theta}\frac{dP_l(x)}{dx} \\ &= -\cos\theta\frac{dP_l(x)}{dx} - \sin\theta[(-\sin\theta)\frac{d}{dx}]\frac{dP_l(x)}{dx} \\ &= -\cos\theta\frac{dP_l(x)}{dx} + \sin^2\theta\frac{d^2P_l(x)}{dx^2}\end{aligned} \tag{B.0.8}$$

$P_l'(x)$ and $P_l''(x)$ are given in Appendix A. The angles θ can be calculated by inverse cosine function of x.

In (B.0.2), there is a 2nd-order differential operator with respect to θ

$$\frac{1}{\sin\theta}\frac{d}{d\theta}(\sin\theta\frac{d}{d\theta}) = \frac{1}{\sin\theta}(\cos\theta\frac{d}{d\theta} + \sin\theta\frac{d^2}{d\theta^2}) \tag{B.0.9}$$

Let the 2nd-order differential operator works on $P_l(x)$. With (B.0.7) and (B.0.8),

$$\frac{1}{\sin\theta}\frac{d}{d\theta}(\sin\theta\frac{dP_l(x)}{dx}) = -2\cos\theta\frac{dP_l(x)}{dx} + \sin^2\frac{d^2P_l(x)}{dx^2}. \tag{B.0.10}$$

The numerical differential with respect to θ only need to perform once.